RESEARCH ARTICLE-EARTH SCIENCES

Characterization of the Gas-Bearing Tight Paleozoic Sandstone Reservoirs of the Risha Field, Jordan: Inferences on Reservoir Quality and Productivity

Sherif Farouk[1] · Abdelrahman Qteishat[2] · Souvik Sen[3] · Fayez Ahmad[4] · Khaled El-Kahtany[5] · Richard Collier[6] · Mohammad A. Sarhan[7]

Abstract

This study presents the petrographical and petrophysical characteristics of the Cambro-Ordovician clastic reservoirs from the Risha field, northeastern Jordan. Routine core analysis, wireline logs, petrographic thin sections, scanning electron microscopy, and X-ray diffraction were integrated to characterize the gas reservoirs of the Risha, Dubeidib, and Umm Sahm formations (the equivalent of Sarah, Qasim, and Upper Saq formations of northern Saudi Arabia). These reservoirs are variably micro- and mesoporous, with permeability < 1 mD and dominantly < 6% porosity. Wireline log-based assessment exhibits low shale volume (< 30%) and high hydrocarbon saturation (45–95%) in these tight reservoirs. Petrographic investigation reveals that these reservoirs are fine-grained sandstones, moderately sorted with high mineralogical maturity. The Risha and Dubeidib reservoirs are subarkose, while the Umm Sahm reservoir is composed of quartz arenite. The late diagenetic silica cementation is inferred as reservoir quality-reducing diagenetic factor, with quartz overgrowth of > 10% corresponding to < 4% porosity. SEM images exhibit the presence of grain-coating, pore-filling, and pore-lining chlorite, and illite phases which hinder quartz overgrowth and had a positive effect in retaining the primary porosity. The sandstones with > 20% clay-coating coverage corresponds to a lower quartz overgrowth (< 5%) and therefore higher intergranular porosity (> 5%). Locally sutured grain contacts and stylolites are observed which indicate intense chemical compaction. The feldspar grains are observed to be partially dissolved, which generated minor secondary porosity. Micropore-dominated pore systems and rare secondary macroporosity are typically isolated by abundant cement and/or pore throats choked by clay minerals.

Keywords Petrography · Diagenesis · Petrophysics · Tight sand · Risha field · Paleozoic tight reservoir

✉ Souvik Sen
  souvikseniitb@gmail.com

1. Exploration Department, Egyptian Petroleum Research Institute (EPRI), 1 Ahmed El-Zomor Street, Nasr City, Cairo, Egypt

2. Chemical Engineering Department, Al-Huson University College, Al-Balqa' Applied University, As-Salt, Jordan

3. Reservoir Technical Services (RTS), Baker Hughes, Mumbai, Maharashtra, India

4. Prince El Hassan Bin Talal Faculty of Natural Resources and Environment, Department of Earth and Environmental Sciences, The Hashemite University, Zarqa, Jordan

5. Geology and Geophysics Department, College of Science, King Saud University, Riyadh, Saudi Arabia
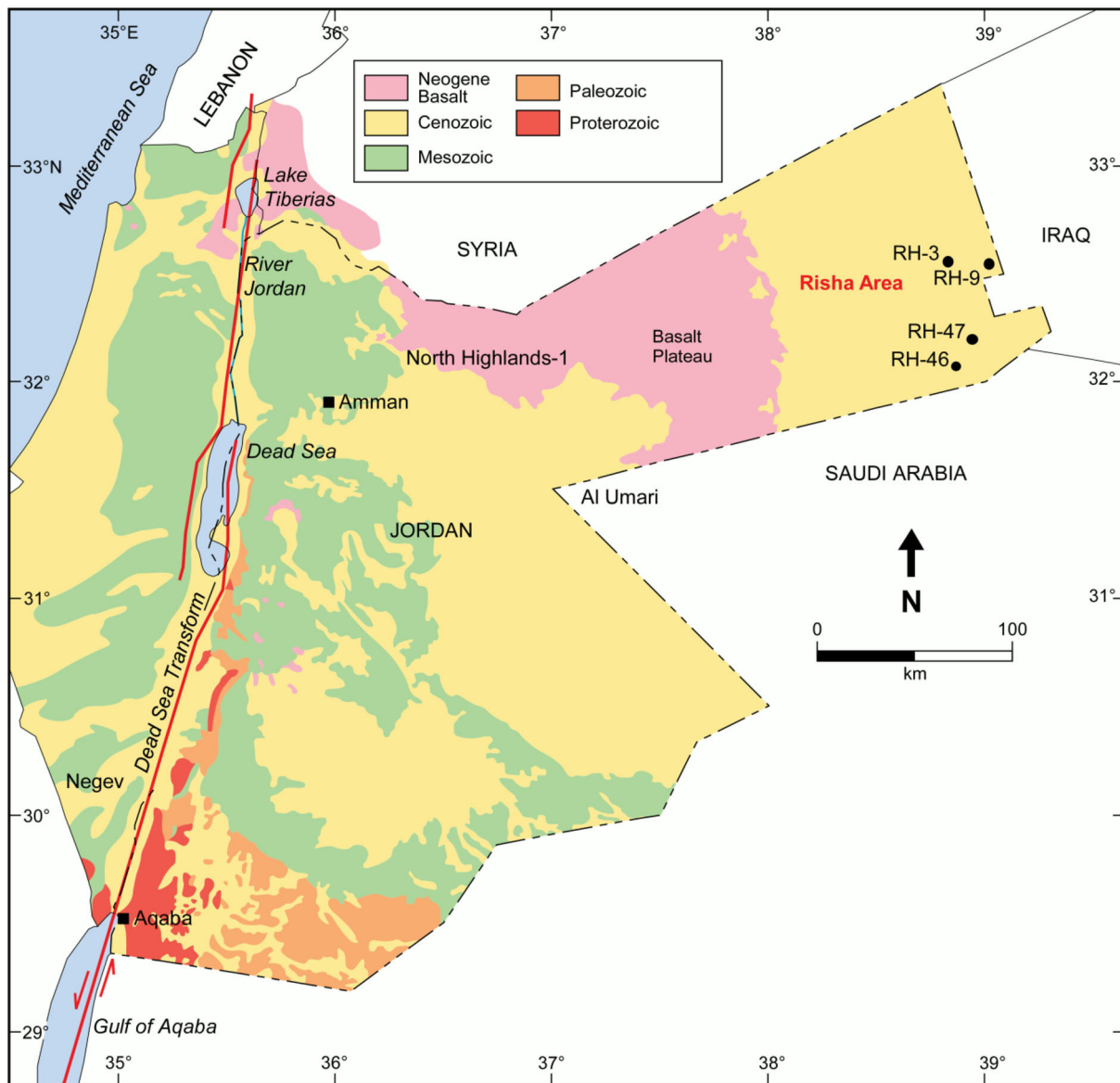
6. School of Earth and Environment, University of Leeds, Leeds LS2 9JT, UK

7. Geology Department, Faculty of Science, Damietta University, Damietta 34517, Egypt

1 Introduction

Tight gas sands account for more than two-thirds of global unconventional production [1]. These refer to low-permeability sandstones that produce dry natural gas [2]. The Middle East and Africa host roughly 823 trillion cubic feet of tight sand gas reserves [1, 3]. The Cambrian-Ordovician glacial sandstones of the Middle East and North Africa hold a large tight sand gas potential. For example, the Paleozoic Hamra Quartzites are one of the most prominent producing reservoir intervals in the Saharan basins of Algeria [4–6]. The Upper Ordovician sandstones of the Sarah Formation are also confirmed as a gas reservoir in central and north-western

Fig. 1 Location map of the Risha gas field, northeastern Jordan, along with the four well locations that have maximum data coverage, modified after Naylor et al. [9]

Saudi Arabia [7, 8]. The present study focuses on the equivalent Paleozoic tight sandstone gas reservoirs of the Risha field, located in the northeastern part of Jordan, near the Iraq border. To maximize the potential of the Lower Paleozoic reservoirs that are part of the petroleum system in Jordan [9], thorough understanding of the properties and hence reservoir quality of targeted pay zones needs to be established.

The Risha field is the most significant gas field in Jordan, presently contributing ~ 5% of domestic natural gas consumption for electricity generation [10]. Production started in 1989, with a total gas reserve of 180 billion cubic feet [11, 12]. Since 2019, Jordan's national oil company has boosted

exploration activity in the eastern desert area to reduce hydrocarbon imports, and the promising gas reserves of the Risha field have become the primary focus. Past field development activities increased Risha production from 8 million cubic feet per day in 2017 to 30 million cubic feet in 2021 from about 30 producing wells. The recent and ongoing activity, which started in 2022, has targeted the drilling of six new wells within the Risha field near the Iraq border to increase the field's production capacity up to 50 million cubic feet per day [13].

The Risha field hosts potential reservoirs in Lower Paleozoic intervals [9], including the deposits of well-stacked
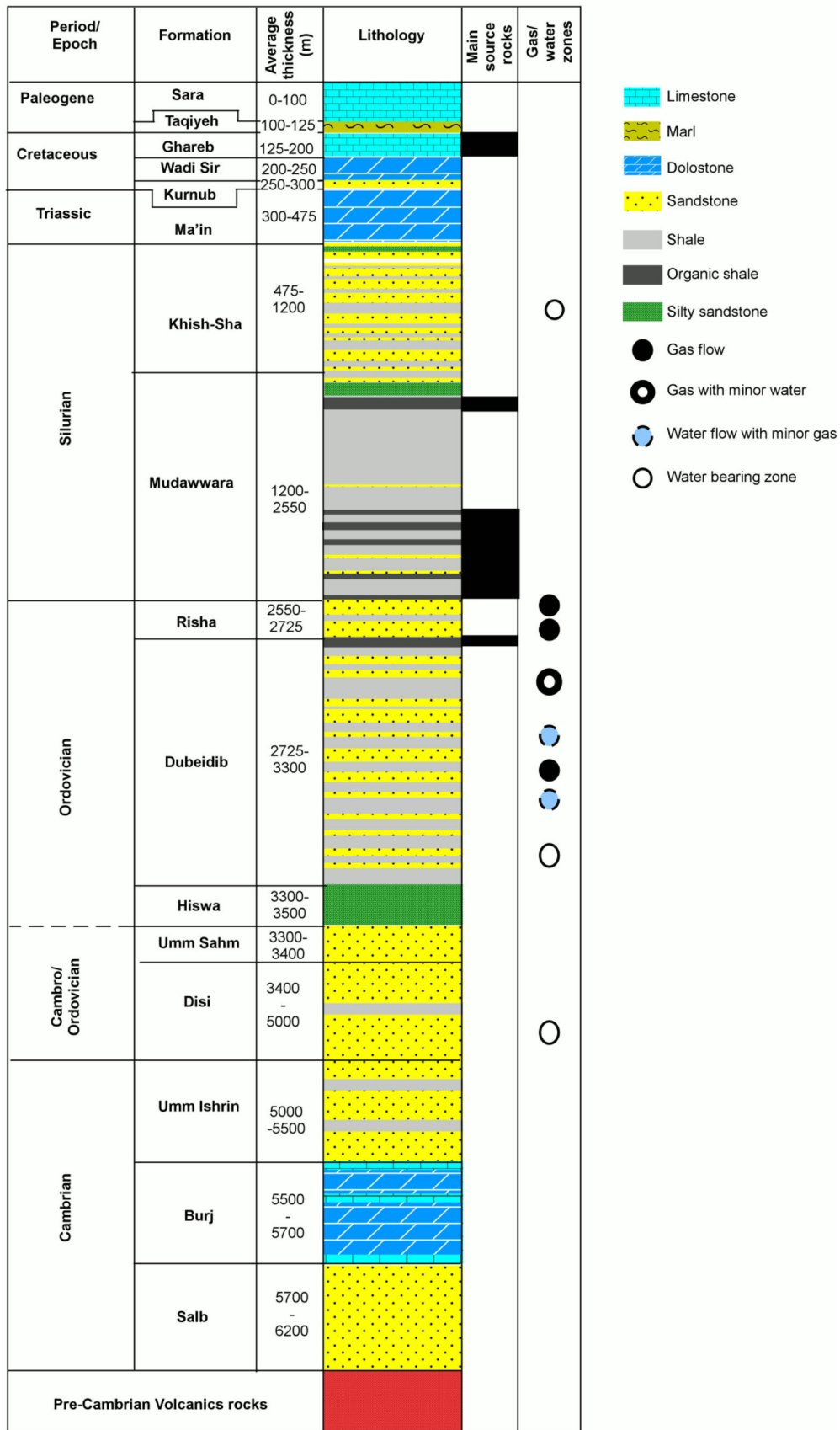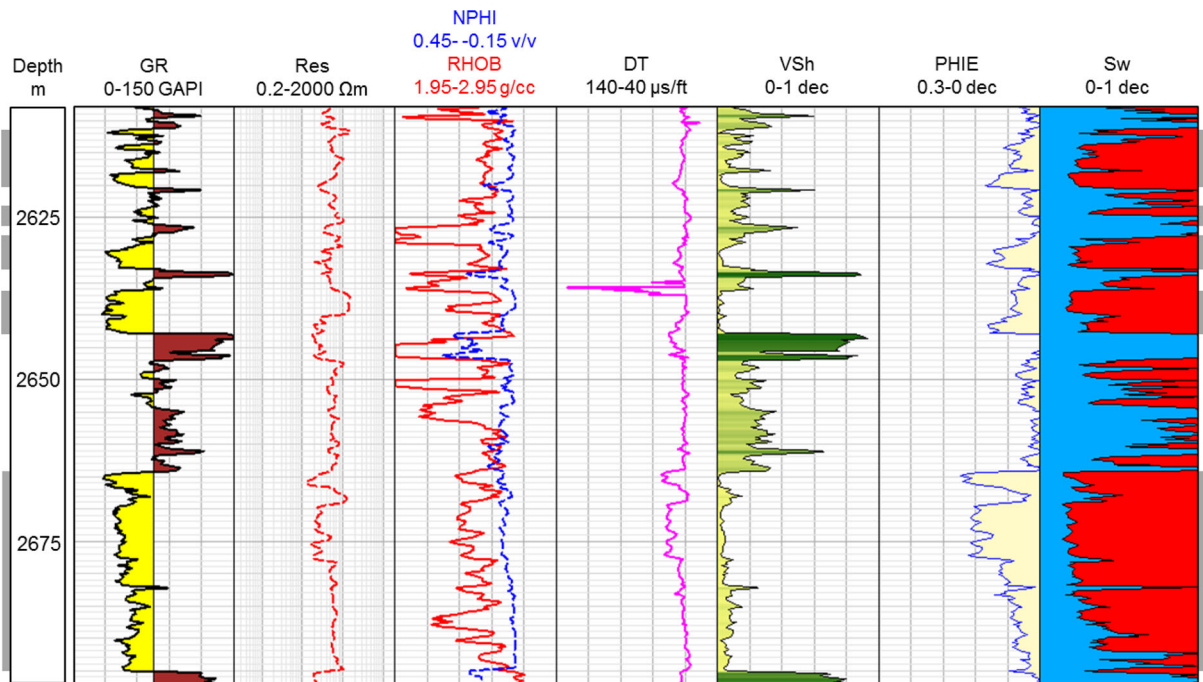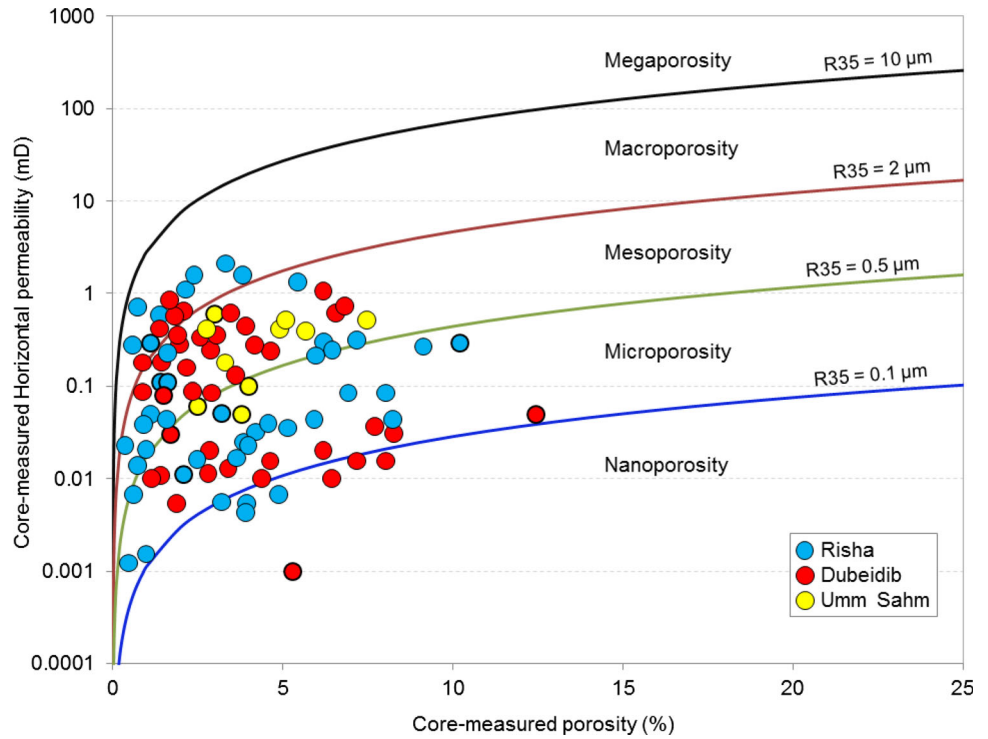
**Fig. 2** Stratigraphic succession of the studied Risha gas field [27]

Fig. 3 Core-based porosity and permeability indicating the dominance of micro- and mesopores within the three studied formations from the Risha field

Fig. 4 Wireline logs and inferred key petrophysical properties of the Risha Formation in the well RH-3. Reservoir pay zones are marked in grey

thin sheets of outwash fan deposits, with sediments delivered via sub-glacial tunnel valleys [14]. Previously published studies from the region have focused on the sequence stratigraphy and depositional environments of Silurian and Ordovician intervals [14–26] and the organic geochemistry, and source rock characteristics of Silurian and Cretaceous shales [22, 27]. Reservoir pore characteristics, the impact of fractures, and reservoir heterogeneity in Upper Ordovician Sarah Formation tight gas sandstones, equivalent to the Risha Formation in Jordan, have been the focus of several studies in Saudi Arabia [8, 28]. However, a comprehensive characterization of reservoir properties and hydrocarbon
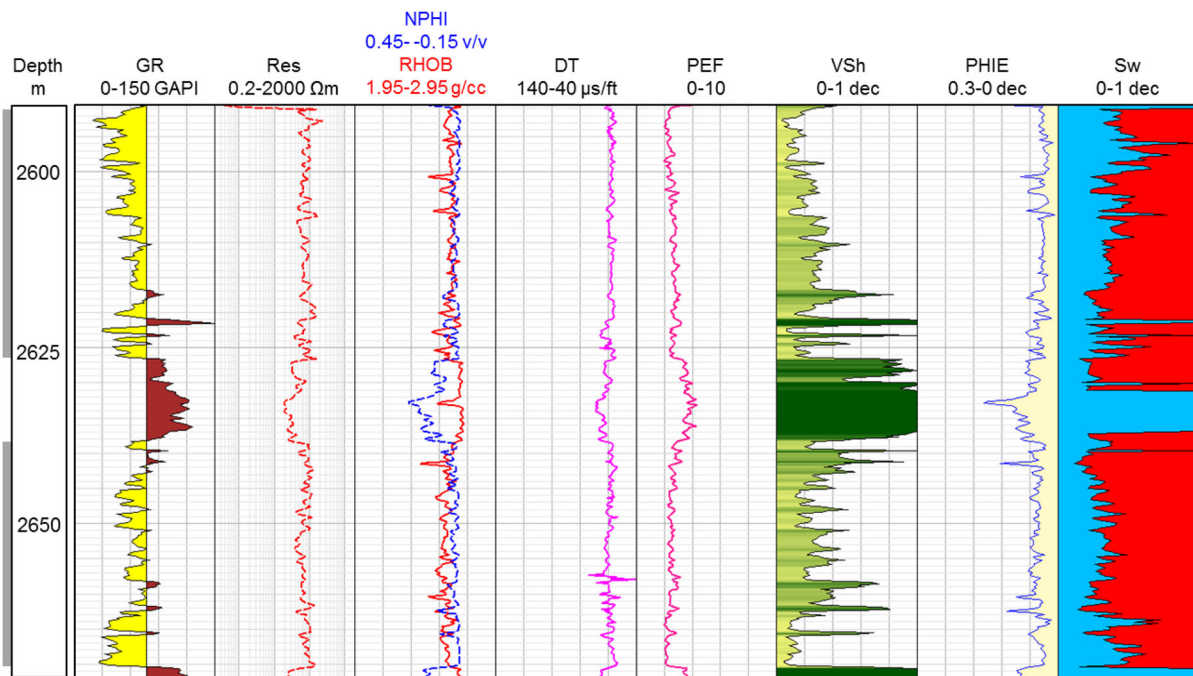
Fig. 5 Wireline logs and inferred key petrophysical properties of the Risha Formation in the well RH-9. Reservoir pay zones are marked in grey

potential of the Lower Paleozoic formations of Jordan has not yet appeared in the published literature. This work integrates information from wireline logs, core-based petrophysical measurements, petrographic thin sections, scanning electron microscopy (SEM), X-ray diffraction (XRD), and drilling data to characterize the Risha, Dubeidib, and Umm Sahm sandstones in the study region. The objectives of this study are to: (i) Infer porosity, permeability, and pore types, (ii) establish key petrophysical properties (effective porosity, shale volume, and water saturation), (iii) describe petrographic characteristics, (iv) characterize mineralogical distribution, and (v) assess the diagenetic processes that have affected the reservoir qualities.

2 Geologic Setting

The studied Risha tight gas field is located on the tectonically active/unstable shelf region of the Arabian plate [29] (Fig. 1). The Tabuk Basin of Saudi Arabia marks its eastern boundary. The studied Risha field is characterized by a low structural dip and hydrocarbon accumulations are characterized by stratigraphic traps, i.e. lateral facies pinch-outs [30]. The major fault systems express this, generally trending south-north or southeast-northeast may have played a role in the initial construction of the tectonics during the Late Precambrian age. Following the Infracambrian extension linked with Pan-African East African-Antarctic Orogeny [31, 32], the Paleozoic remained tectonically inactive. Compressional

tectonics took place during the Late Carboniferous, which resulted in the uplift and erosion of the Upper Paleozoic sediments during the Hercynian Orogeny [33] as well as the reactivation of key structural trends.

A general lithostratigraphic column is presented in Fig. 2. The basin hosts Cambrian-Eocene sediments approximately 6 km thick, directly above the Precambrian volcanic basement [34]. Cambro-Ordovician sedimentation (Ram Group) is dominated by terrestrial to shelf marine siliciclastics [16, 35], of which the Umm Sahm Formation is the uppermost unit. The Cambrian Salb, Umm Ishrin, and Disi formations of the Ram Group are dominated by a long-lived and extensive braid plain with clastics deposited by northward-flowing streams, except for the mid-Cambrian Burj Formation marine carbonates which represent the first Paleozoic marine transgression in the region [35]. The Upper Cambrian-Ordovician is composed of marine and non-marine sandstone-shale sequences and hosts the primary gas reservoirs of the Risha field [14, 36]. The Disi and Umm Sahm formations of the Upper Cambrian to Ordovician Ram Group include fluvial, braided channel sandstones but are interbedded with a variety of shallow marine and tidally influenced sediments [35].

The Middle-to-Upper Ordovician Dubeidib Formation, equivalent to the Qasim Formation in NW Saudi Arabia [14] comprises marine argillaceous to sandy, storm-dominated shoreface deposits which show characteristic cleaning-up,
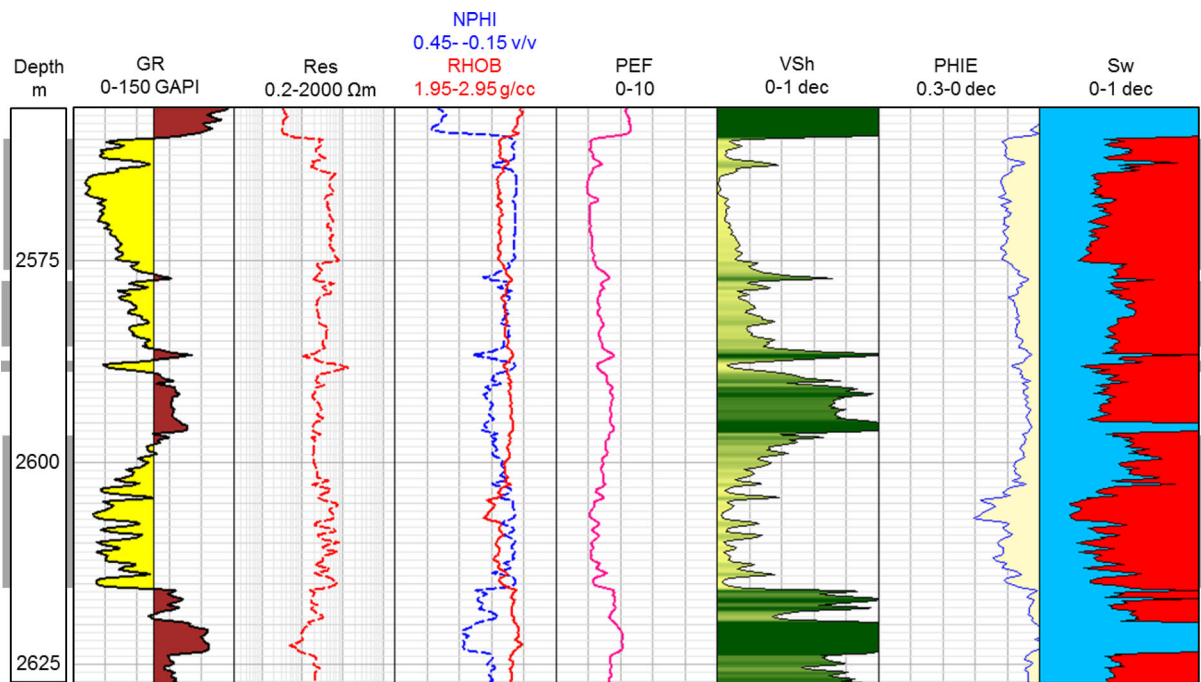
Fig. 6 Wireline logs and inferred key petrophysical properties of the Risha Formation in the well RH-46. Reservoir pay zones are marked in grey

coarsening-upwards cycles forming a hierarchy of progradational sequences and parasequence [37]. These shallowing-up packages are laterally extensive parallel to the northern Gondwana continental margin.

The Risha Formation, equivalent to the Ammar Formation in southern Jordan and the Sarah/Zarq Formation in Saudi Arabia [14], represents significant erosional and depositional events related to Hinantian (Upper Ordovician) glacio-eustatic fluctuations and associated growth and decay of the Gondwanan ice sheet [14]. In southern Jordan and parts of NW Saudi Arabia, incised valleys are interpreted as sub-glacial tunnel valleys [24] formed during ice expansion and glacio-eustatic low stand conditions. These valleys are in the order of 1000 m wide and > 100 m deep [14]. They are interpreted to have supplied sands to the north where the resulting stacked sandstone sheets can be correlated over tens of kilometres and are therefore interpreted as stacked glacial outwash fan deposits. In northern Jordan, the lower part of the Risha Formation infill of each valley commonly shows a fining-up, dirtying-up retrogradational trend indicating transgression associated with ice sheet retreat, but with the overall retrogradational trend incorporating individually coarsening-up parasequences. Maximum flooding occurs in the Risha II unit of the Hirst & Khatatneh [14] scheme. Above this, there is typically a progradational parasequence set to the top of the Risha Formation, interpreted as recording the progressive filling and oceanward regression of shallow marine to fluvial facies along the remnant incised valleys. Erosion driven by a glacial rebound in the hinterland, as the ice sheet retreated,

possibly associated with the reactivation of NW–SE trending faults, may have enhanced sediment supply during this progradational phase.

A significant transgression led to the deposition of Mudawwara Formation shale all over Jordan, as a result of the end of Ordovician glacial activity and the melting of ice by the Early Silurian [24, 25]. The Silurian shales of the Mudawwara Formation are the primary source rocks [34] of the region. Where the hot shales of the Mudawwara Formation are buried more deeply, they represent mature shales from which dry gas has been generated [34].

The top of the Silurian Khisheh Formation marks a regional unconformity that separates the Paleozoic clastics from Mesozoic dolomites [34]. This unconformity demonstrates how the Upper Paleozoic was eroded in response to Hercynian uplift and hence is missing in the studied area. The Triassic, Cretaceous, and Paleogene intervals are dominated by carbonate deposits linked to the sea level rise of the Tethys Ocean and the development of a major carbonate platform over a large area [30, 38, 39]. In addition to the Mudawwara Formation shales, other organic-rich shales are present in the Late Ordovician and Late Cretaceous intervals.

3 Data and Methods

This study utilizes wireline logs, routine core analysis (RCAL), petrographic thin sections, SEM, XRD, and drilling data to characterize the reservoir characteristics of the Risha,
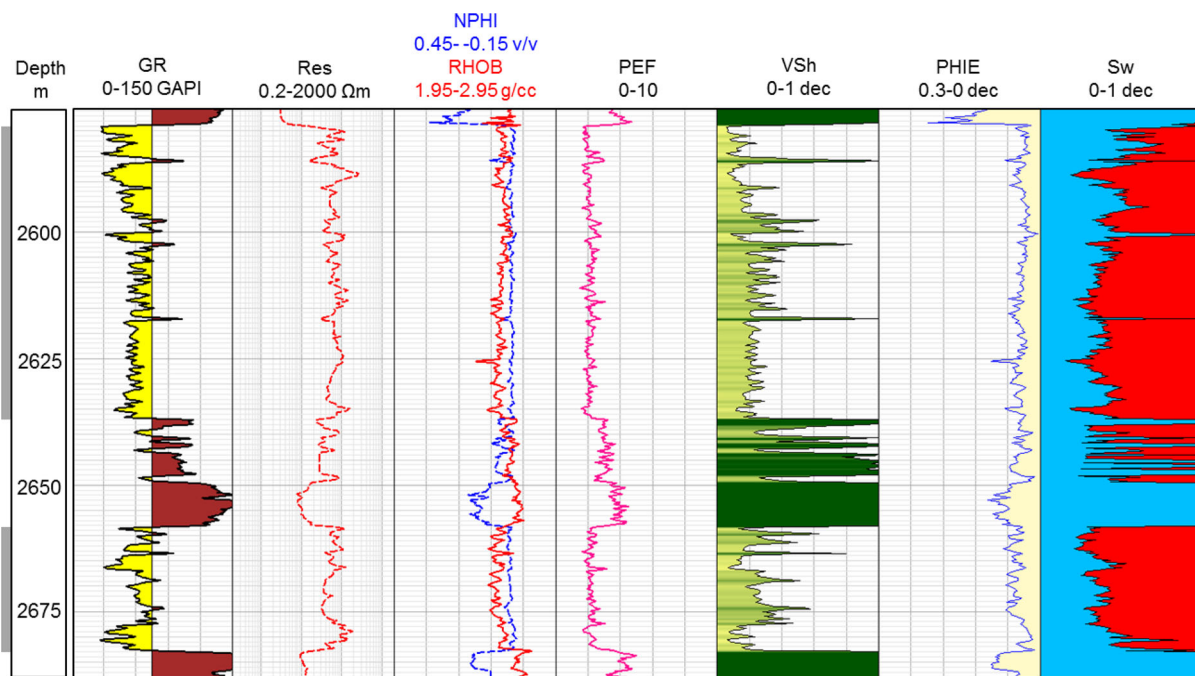
Fig. 7 Wireline logs and inferred key petrophysical properties of the Risha Formation in the well RH-47. Reservoir pay zones are marked in grey

Dubeidib, and Umm Sahm formations. RCAL provided porosity and horizontal permeability measurements. Based on data availability, completeness, and formation coverage, four wells were chosen for log-based quantitative petrophysical assessments, which are RH-3, RH-9, RH-46, and RH-47. The wireline log suite includes gamma ray (GR), deep resistivity (Res), bulk density (RHOB), and neutron porosity (NPHI), which were utilized to estimate shale volume (Vsh), effective porosity (PHIE), and water saturation (Sw). The latter was estimated using gamma-ray (GR) log data [40]:

$$\mathrm{Vsh} = \frac{\mathrm{GR} - \mathrm{GRmin}}{\mathrm{GRmax} - \mathrm{GRmin}} \tag{1}$$

GRmin and GRmax are the minimum and maximum gamma-ray values in a particular formation interval, respectively. PHIE was estimated based on Vsh, NPHI, and density-derived total porosity. Sw was inferred following the Indonesian model [41]:

$$\mathrm{Sw} = \left\{ \frac{\sqrt{\frac{1}{\mathrm{Res}}}}{\left\{ \left(\frac{\mathrm{Vsh}^{1-0.5\,\mathrm{Vsh}}}{\sqrt{\mathrm{Rsh}}} \right) + \sqrt{\frac{\Phi e^m}{a\mathrm{Rw}}} \right\}} \right\}^{\frac{2}{n}} \tag{2}$$

Rsh = shale resistivity, taken as 5 Ωm; Rw = resistivity of the connate water, taken as 0.03 Ωm; 'a' is tortuosity factor (considered $a = 1$); 'm' and 'n' are cementation exponent and saturation exponents, respectively, with an assumed value of

2. Due to the tight nature of the sandstones, a porosity cut-off of 5% was considered to distinguish reservoir pay zones along with 30% Vsh and 55% Sw cutoffs. Lithology and hydrocarbon effects were analysed from the RHOB-NPHI cross-plot. Spectral gamma-ray data were recorded in the well RH-47, which provided thorium (Th) and potassium (K) concentration. A cross-plot between 'Th' and 'K' was utilized to infer clay mineralogy.

A total of 20 thin sections were prepared from selected core samples and examined using an Olympus BX53P petrographic polarizing microscope. The thin sections were impregnated with blue-dyed resin to facilitate the porosity identification. The staining methods by Dickson [42] were followed, using a mixed Alizarin Red-S and Potassium Ferri Cyanide solution to identify the carbonate minerals in the studied samples. Petrographic thin sections of the three reservoirs were available from the wells RH-23, RH-25, and RH-47. Out of 25 thin sections, 10 were available from the Risha Sandstone reservoirs, and 5 each from the Dubeidib and Umm Sahm reservoirs. Based on the modal point count analysis of 200 counts per thin section, the constituting detrital components, cement and clay minerals, and pore types were inferred. Clay-coating coverage (in %) was estimated following the method proposed by Dutton et al. [43]. Scanning electron microscopy (SEM) analysis was carried out on a total of 10 samples using a Quanta FFG-450 SEM instrument in Jordanian Nanotechnology Institute. SEM photographs were available only for the Risha Formation in the well RH-29, which provided high-resolution
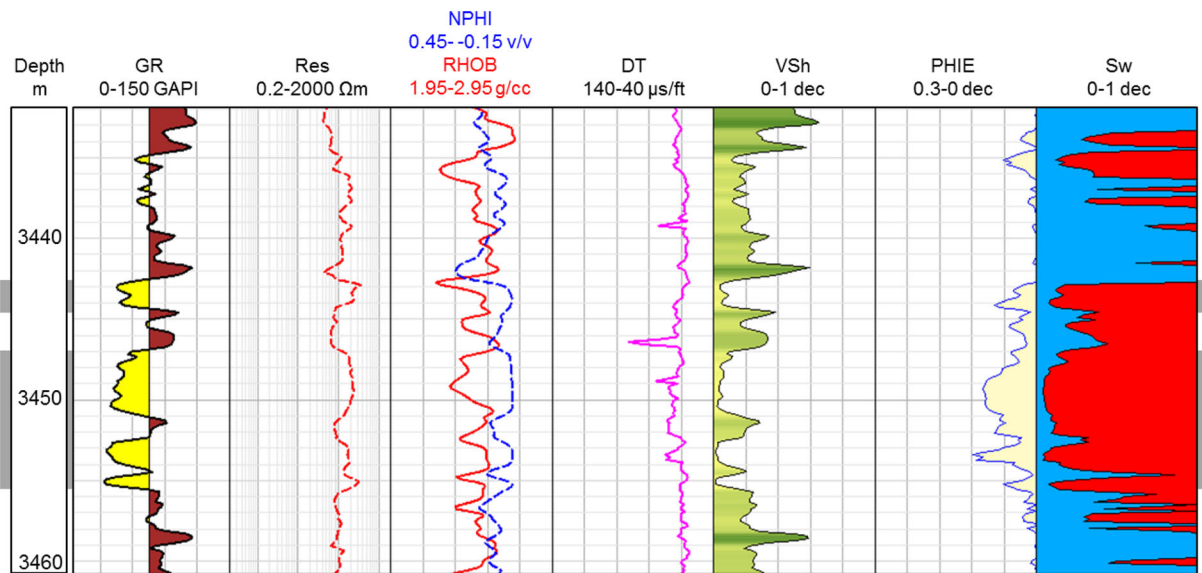
Fig. 8 Wireline logs and inferred key petrophysical properties of the Dubeidib Formation in the well RH-3. Reservoir pay zones are marked in grey
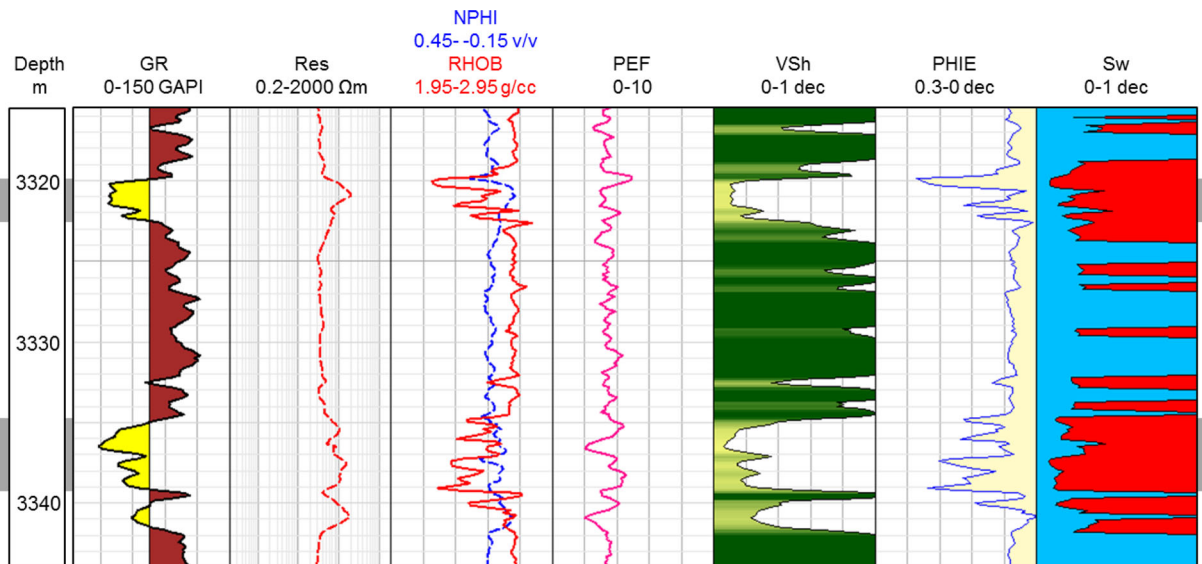
Fig. 9 Wireline logs and inferred key petrophysical properties of the Dubeidib Formation in the well RH-47. Reservoir pay zones are marked in grey

information about the cement and clay mineralogy and their distribution. Based on the thin section and SEM evaluations, diagenetic factors were inferred together with their effects on reservoir quality. XRD data yielded further information on the whole-rock composition and clay fraction. XRD analysis was performed on a total of 33 samples, which include 23 samples from the Risha Formation, 7 from the Dubeidib Formation, and 3 from Umm Sahm Formation. A Bruker D8 advance diffractometer was utilized to conduct XRD analysis which provided the whole-rock composition. This is a destructive analysis technique involving grinding a small rock sample (around 10 g) to a fine powder for whole-rock analysis. Drilling reports were available from the two wells RH-7 and RH-16, which were the best gas-producing wells in the Risha field. Drilling loss events (number of events, loss rate, and cumulative mud loss volume) were summarized the possible effects of fractures on reservoir productivity.
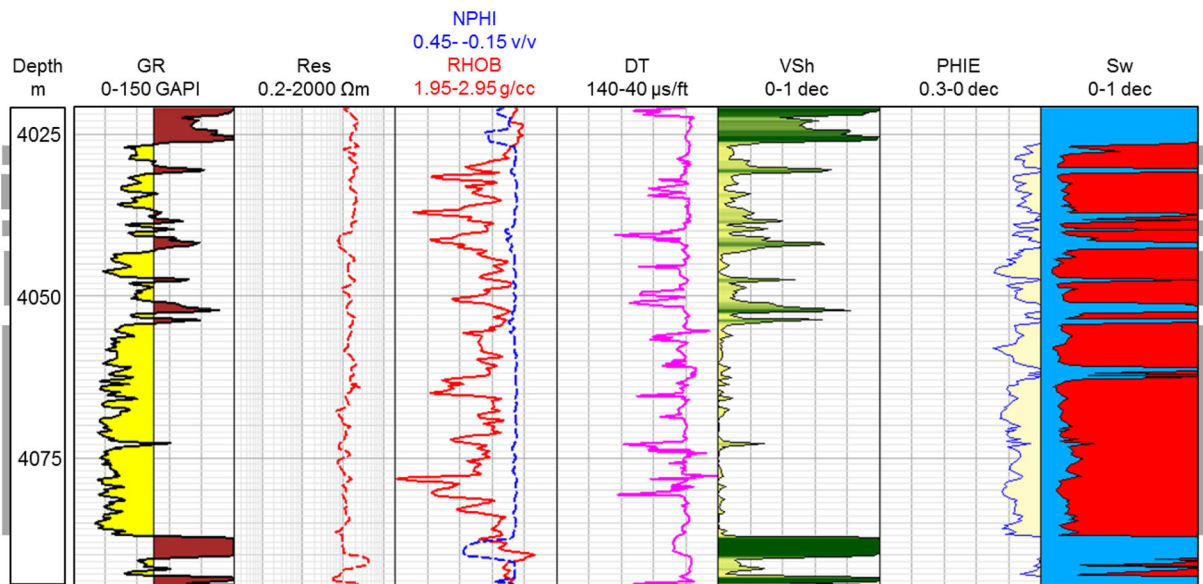
Fig. 10 Wireline logs and inferred key petrophysical properties of the upper Umm Sahm Formation in the well RH-3. Reservoir pay zones are marked in grey
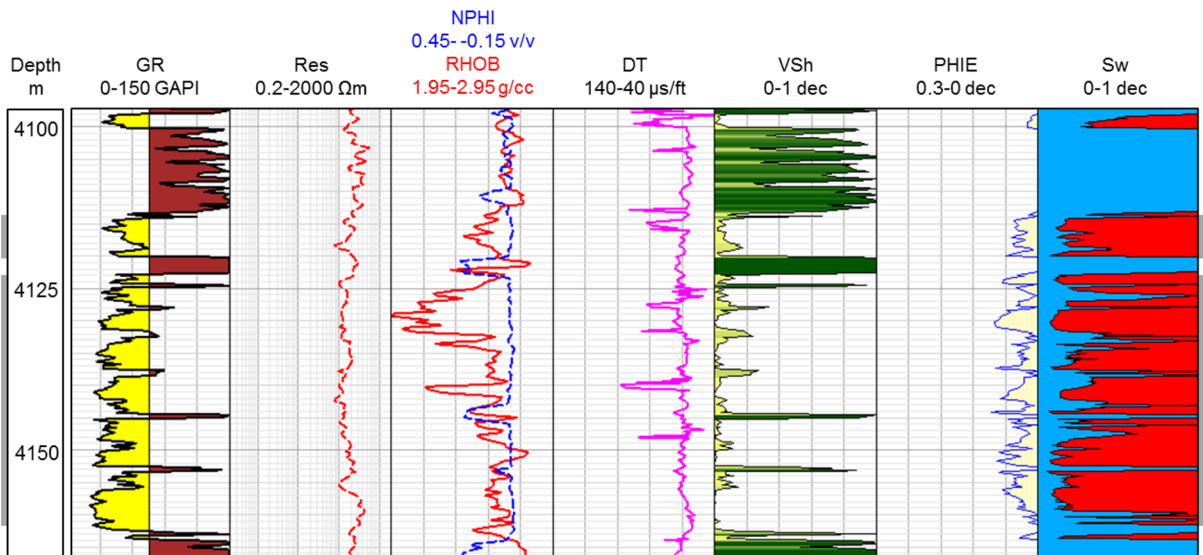

Fig. 11 Wireline logs and inferred key petrophysical properties of the lower Umm Sahm Formation in the well RH-3. Reservoir pay zones are marked in grey

4 Results

4.1 Petrophysical Analysis

The quantitative and qualitative petrophysical assessments of the Risha, Dubeidib, and Umm Sahm formations were performed based on the core measurements and wireline log analysis. An RCAL-based porosity against permeability cross-plot is presented for the three formations in Fig. 3. The data are quite scattered, and a confident poro-perm relationship could not be achieved; however, the majority of the data distribution indicates horizontal permeability of less than 1 mD and porosity ranging between 1 and 10%, dominantly < 6% (Fig. 3). This is indicative of the very tight nature of all the three Paleozoic intervals. Following the Winland model-based pore throat radius (R35) estimates, we infer 0.1 μm ≤ R3 ≤ 2 μm, which satisfies the majority of the data distribution. This inferred R35 range indicates the dominance of micro- and mesoporosities. Careful observation indicates that the Umm Sahm Formation primarily demonstrates of mesoporosity (Fig. 3).
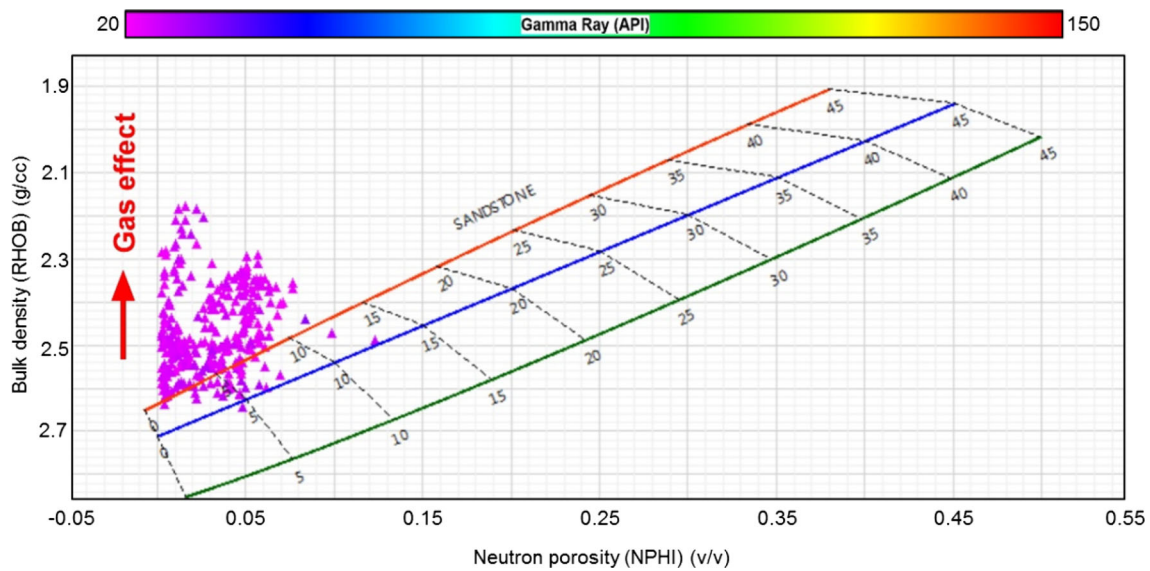
Fig. 12 Cross-plot between neutron porosity and bulk density indicating lithological compositions and gas effects in the Risha Formation pay zones from the well RH-3
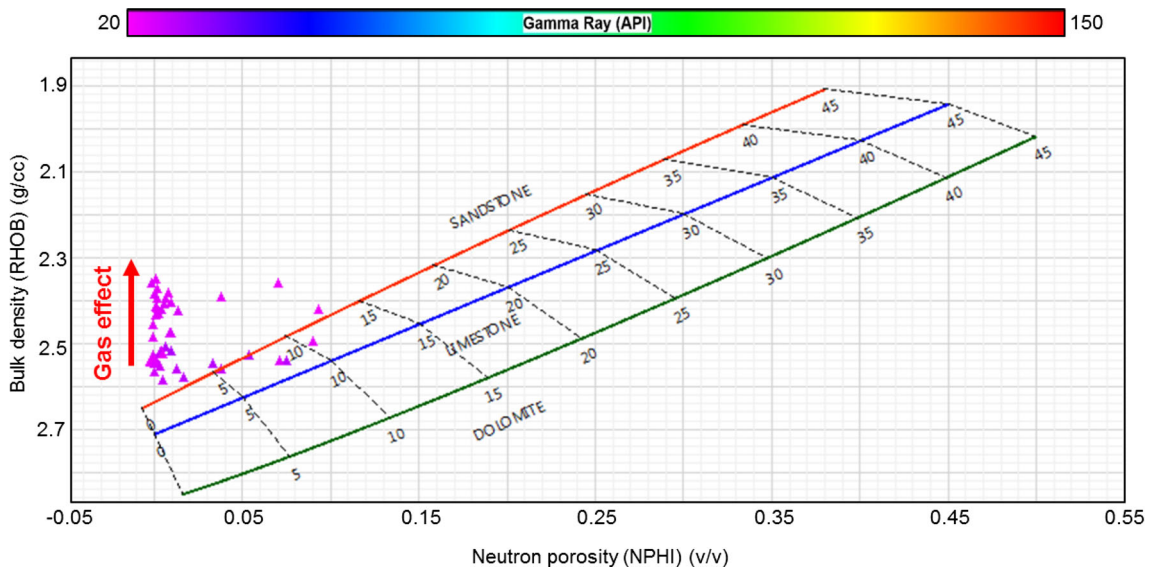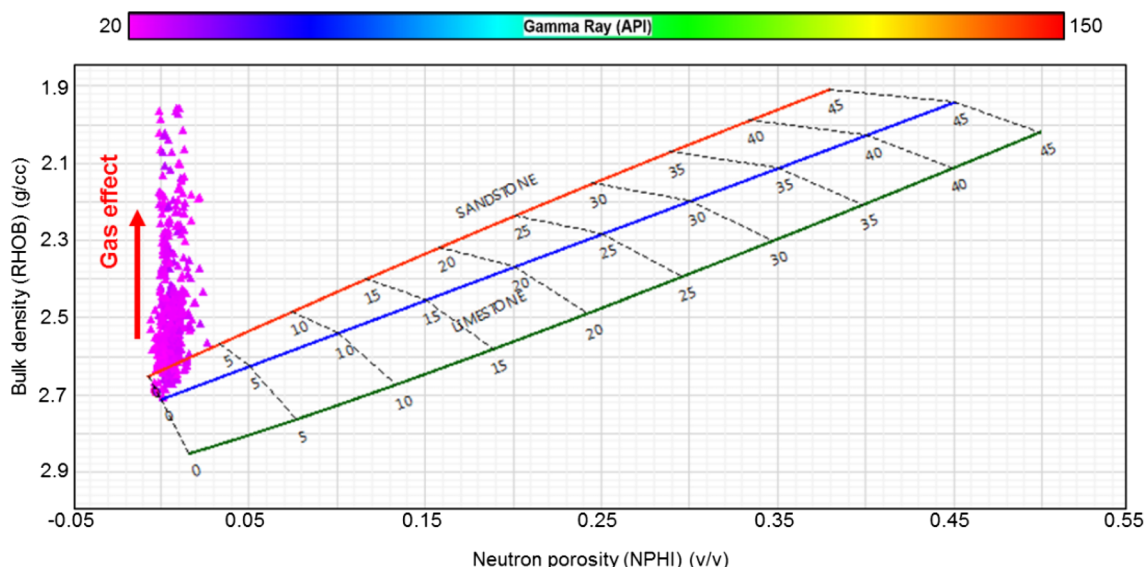

Fig. 13 Cross-plot between neutron porosity and bulk density indicating lithological compositions and gas effects in the Dubeidib Formation pay zones from the well RH-3

Based on the wireline log data coverage, we analysed the key petrophysical properties of the Risha Formation from four wells, i.e. RH-3 (2610–2695 m, Fig. 4), RH-9 (2590–2670 m, Fig. 5), RH-46 (2560–2615 m, Fig. 6), and RH-47 (2580–2680 m, Fig. 7). The promising reservoir intervals in the Dubeidib Formation are located between depths of 3442–3456 m in the RH-3 well (Fig. 8) and 3320–3341 m in the RH-47 well (Fig. 9). Potential Umm Sahm reservoir sands were identified in RH-3 between 4025 and 4085 m (upper zone, Fig. 10) and 4115–4160 m (lower zone, Fig. 11).

Based on the gamma-ray cutoff of ~ 75 GAPI, the Risha reservoir zones in all four wells (RH-3, RH-9, RH-46,

and RH-47) indicate two clean sand intervals separated by 10–20 m of shales, which demarcates a vertical flow barrier (Figs. 4, 5, 6 and 7). The interpreted hydrocarbon-bearing zones in the three formations are characterized by the small amount of shale volume, which is evidenced by the low gamma-ray (GR < 75 GAPI), along with high deep resistivity (Res ~ 200 Ωm) and the cross-over between neutron porosity and bulk density indicating presence of gas. The gas effect was also observed in the density-neutron cross-plots from all three studied formations (Figs. 12, 13 and 14), where the majority of the data points are clustering around and above the sandstone line, indicating a sandy matrix. These reservoir

Fig. 14 Cross-plot between neutron porosity and bulk density indicating lithological compositions and gas effects in the Umm Sahm Formation pay zones from the well RH-3

Table 1 Summary table for the estimated key petrophysical properties of the promising reservoir intervals from the three studied formations

Formation	Well name	Reservoir Interval (m)		Thickness (m)	Vsh	PHIE	Sw	Sh	Figure no.
		From	To		dec	dec	dec	dec	
Risha	RH-3	2610	2695	85	3–10	6–15	15–35	65–85	4
	RH-9	2590	2670	80	5–30	6–10	25–40	60–75	5
	RH-46	2560	2615	55	5–20	6–12	20–55	45–80	6
	RH-47	2580	2680	100	5–20	5–10	35–55	45–65	7
Dubeidib	RH-3	3442	3456	14	2–5	5–10	5–10	90–95	8
	RH-47	3320	3341	21	10–20	6–12	10–20	80–90	9
Umm Sahm	RH-47 Upper zone	4025	4085	60	2–5	5–7	10–20	80–90	10
	RH-47 Lower zone	4115	4160	45	0–5	4–6	15–25	75–85	11

Vsh shale volume, *PHIE* effective porosity, *Sw* water saturation, *Sh* hydrocarbon saturation

zones exhibit 3–30% shale volume, 4–15% effective porosity (PHIE), 5–55% water saturation, and 45–95% gas saturation (Table 1).
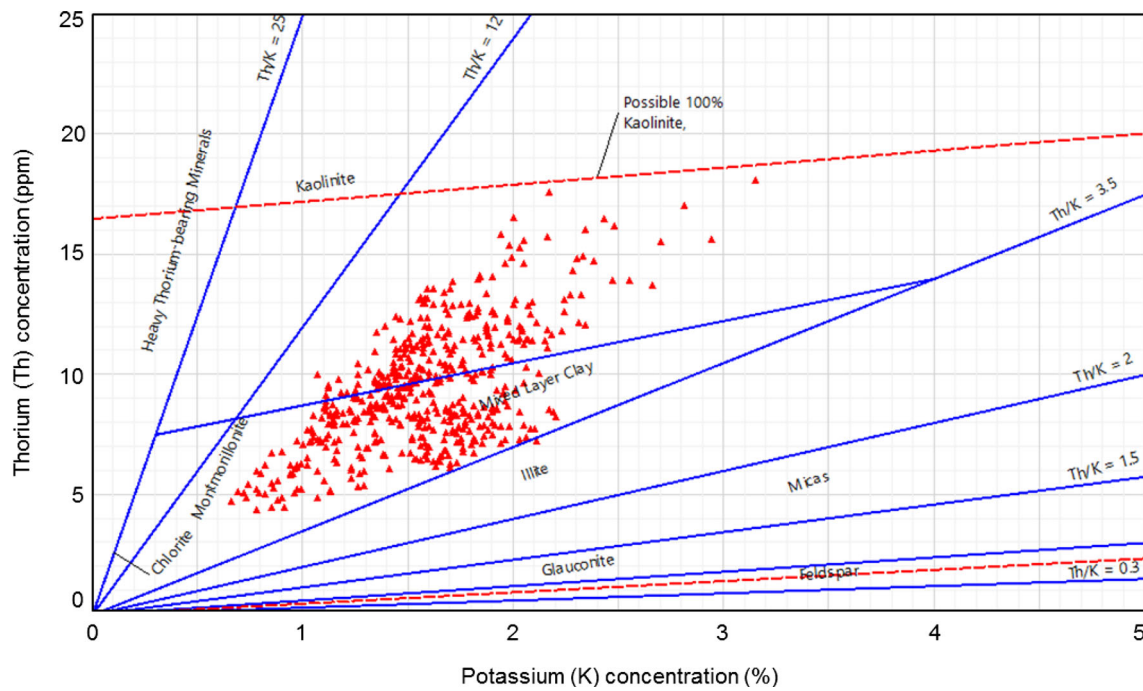
The potassium-thorium concentrations available from spectral gamma-ray data of the Risha and Dubeidib intervals display mixed-layer clay and montmorillonite as the dominant clay phases in the examined wells (Figs. 15, 16).

4.2 Petrographic Investigation

The Risha Sandstone is light–dark grey, very hard, brittle, and dominantly composed of very fine-to-fine, sub-angular to sub-rounded, moderately sorted quartz grains along with subordinate amounts of K-feldspar, trace amounts of mica and heavy minerals (Fig. 17a–d). The silica cementation is commonly observed in all the Risha Sandstone (up to 12% in the Risha Sandstone and up to 18% in the Umm Sahm Sandstone, based on the point count data) that filled the pore spaces (Fig. 17b–c). Pore-filling carbonate cement (i.e. dolomite, Fig. 17b–c), diagenetic clay filling (Fig. 17d), and chlorite rims surrounding the quartz grains (Fig. 17b–d) are commonly observed in all the thin sections. The framework grains are tightly packed with very minor interparticle macroporosity. The feldspar grains are observed to be partially altered and dissolved (Fig. 17c–d).

The SEM images of the Risha Sandstone exhibit the presence of chlorite and illite clay phases which mostly occur as grain-coating, pore-filling, and pore-lining forms (Fig. 18a–c). Chlorite fills are coarser in the central part of the pores than the peripheries (Fig. 18a). Carbonate (Fig. 18d)

Fig. 15 Cross-plot between potassium (K) and thorium (Th) concentrations indicating montmorillonite, kaolinite, and mixed-layer clay as the dominant clay phases within the Risha Formation pay zones from the well RH-47
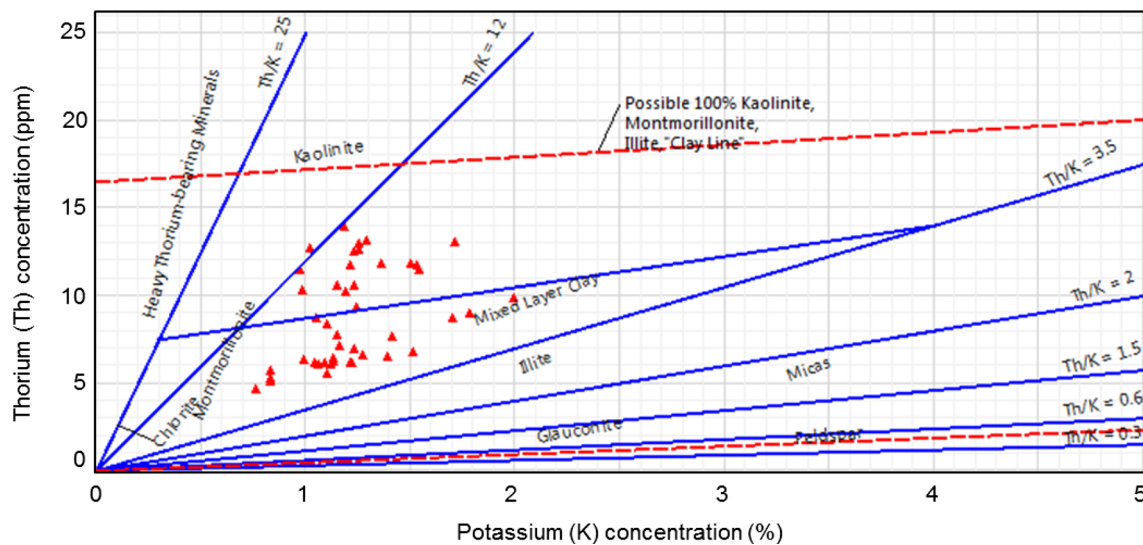

Fig. 16 Cross-plot between potassium (K) and thorium (Th) concentrations indicating montmorillonite, kaolinite, and mixed-layer clay as the dominant clay phases within the Dubeidib Formation pay zones from the well RH-47

and quartz (Fig. 18b) cementation are also observed in SEM. Carbonate cements exhibit developed cleavage planes (Fig. 18d).

The Dubeidib reservoirs are composed of mostly argillaceous sandstones with siltstones and clay interbeds. In thin sections, the argillaceous sandstone exhibits a starry night appearance characterized by very fine-grained quartz and laminated clay fabrics (Fig. 19a). Quartz is the dominant framework grain, followed by plagioclase and K-feldspars.

Partially altered feldspars and pore-filling clay are observed along with minor dolomites (Fig. 19b). Grain-coating chlorite rims are observed. Primary interparticle porosity and minor intraparticle porosity created by feldspar dissolution are observed in the Dubeidib Sandstone samples.

The Umm Sahm Sandstone is primarily composed of fine-to-medium-grained, moderately well-sorted quartz with traces of heavy minerals (Fig. 20a–b). Locally sutured grain contacts and stylolites are observed (Fig. 20a). Umm Sahm
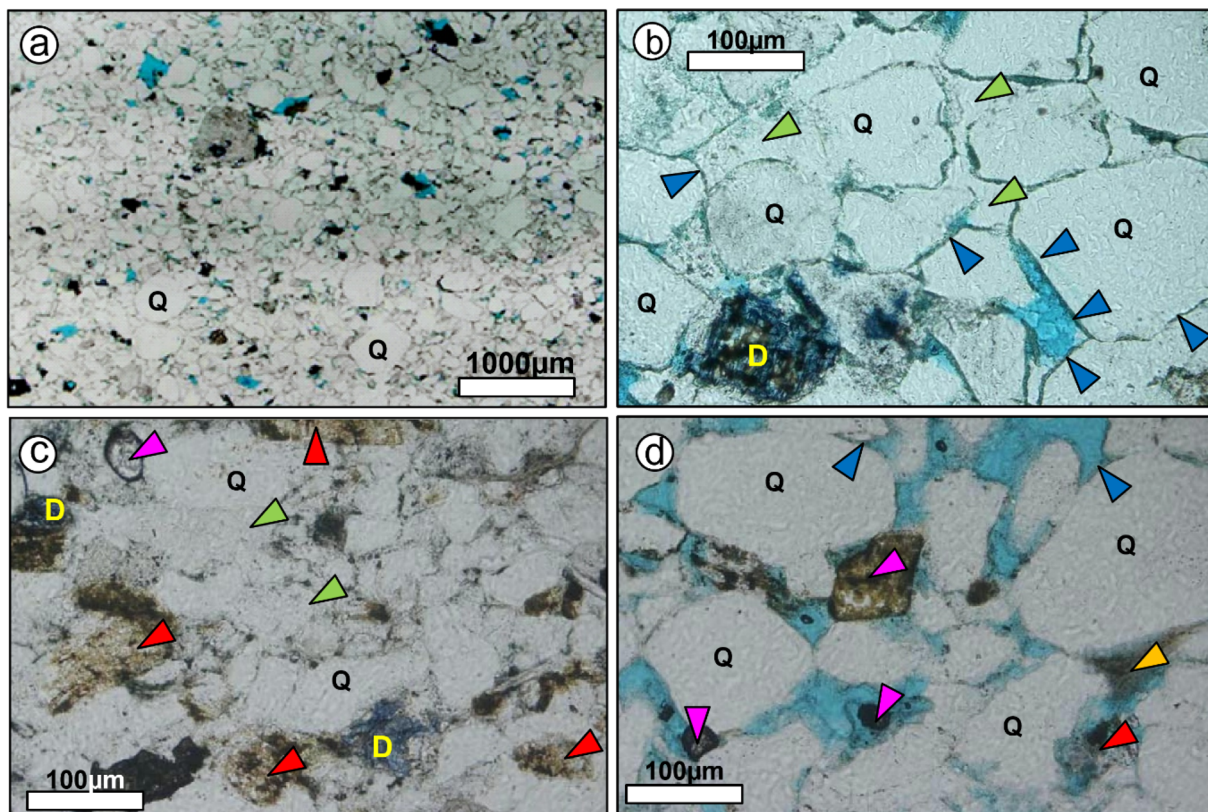
Fig. 17 Optical photomicrographs of the Risha Formation (reservoir pay zones) from **a–b** depth 2635.95 m, well Risha-23, **c** depth 2660.25 m, well Risha-25 and **d** depth 2677.53 m, well Risha-25, indicating the dominant quartz grains (Q), subordinate amount of fresh to partially altered/dissolved feldspar (red arrow), pore-filling detrital clay (orange arrow), chlorite rims surrounding quartz framework grains (blue arrow), minor ferroan dolomite (D) and extensive pore-filling quartz cement (green arrow), along with trace amounts of heavy minerals (pink arrow). Primary interparticle macropores are present (impregnated with blue-dyed resin)

Sandstone exhibits extensive quartz cementation in all samples (up to 18% based on point count data). The chlorite rims around quartz grains and minor pore-filling detrital clay materials are also observed, comparatively lesser than the Risha and Dubeidib samples. Micropore-dominated pore systems and rare secondary macroporosity are typically isolated by abundant cement and/or choked by clay minerals.

The QFR plot is presented in Fig. 21, based on the sandstone classification system by Folk [44]. Compositionally the Risha and Dubeidib sandstones are arkose and Umm Sahm Sandstone is quartz arenite (Fig. 21). The XRD results are presented in Fig. 22, which specify that quartz is the dominant mineral phase in all three formations, followed by feldspar with minor carbonate and siderite. The quartz percentage is highest in the Umm Sahm Sandstone (Fig. 22a), while the Dubeidib Sandstone contains a higher concentration of feldspar when compared with the other two formations (Fig. 22b). The Umm Sahm interval is almost devoid of feldspars and carbonates. The clay content is highest in the Dubeidib Formation and lowest in the Umm Sahm Formation, as was also observed in the thin sections. Chlorite and illite are the dominant clay phases, as identified in XRD as well as SEM.

5 Discussion

5.1 Diagenesis of the Paleozoic Reservoirs

All the three studied reservoir intervals exhibit very strong diagenetic imprints which significantly influenced the intergranular porosity of the studied sandstones. Compaction, cementation, and feldspar dissolution are identified as the three diagenetic processes affecting the Paleozoic reservoir quality in the Risha tight gas field. The paragenetic sequence is presented in Fig. 23. Following deposition, the sandstones were compacted, that resulted in tighter grain packing. Mechanical compaction continued throughout the burial. Mechanical compaction is evident based on the concavo-convex and long straight grain contacts (Fig. 17b, d) as well as the overall tight packing of quartz grains. During the early diagenetic phase, grain-coating chlorite rims were
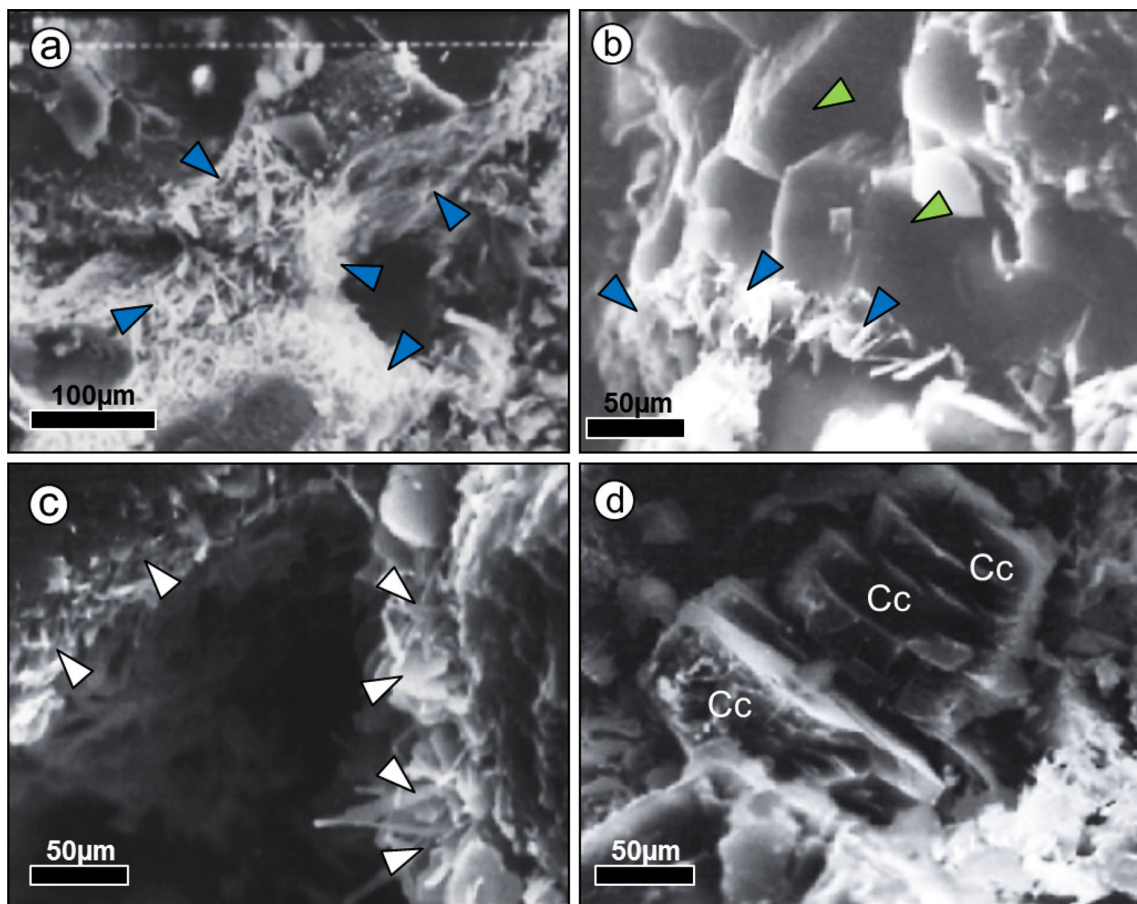
Fig. 18 **a–d** Scanning electron microscope (SEM) images of the Risha sandstones from the well RH-29 at a depth of 2684.7 m indicating pore-filling, grain-coating, and pore-lining chlorites (blue arrow), quartz cementation (green arrow), pore-lining illite (white arrow), and carbonate cement (Cc)
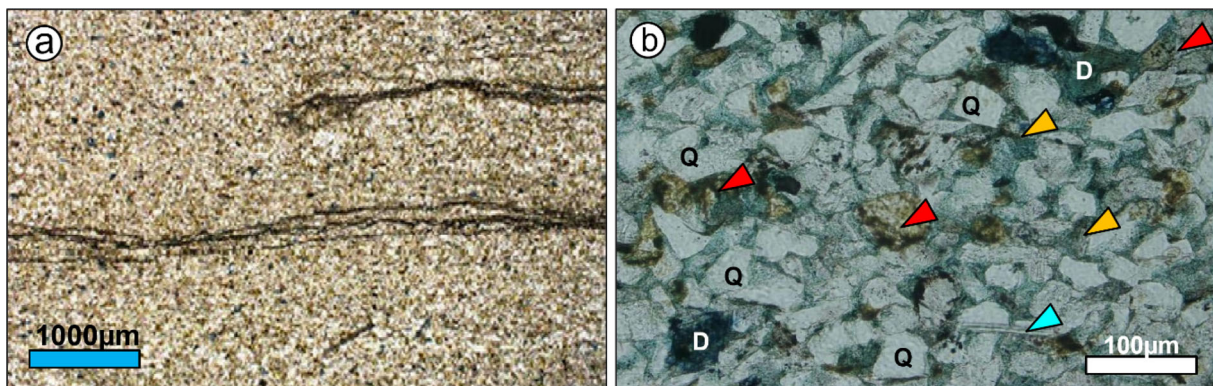

Fig. 19 Optical photomicrographs of the Dubeidib Formation (reservoir pay zones) from **a** depth 3335.03 m, well RH-47 exhibiting very fine-grained sandstone–siltstone with laminated clay fabric and starry night appearance, **b** depth 2939.55 m, well Risha-23, indicating abundant quartz grains (Q), subordinate amount of fresh to partially altered/dissolved feldspar (red arrows), pore-filling detrital clay (orange arrows), and minor ferroan dolomite (D) along with trace amounts of mica (aqua blue arrow)
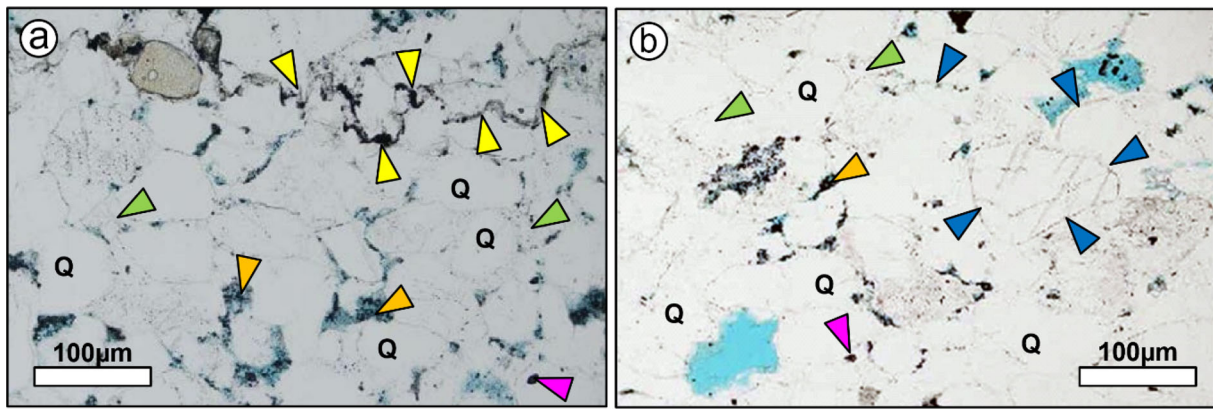
Fig. 20 Optical photomicrographs of the Umm Sahm Formation (reservoir pay zones) from **a** depth 4292.7 m, and **b** depth 4191.5 m, well RH-47, indicating abundant quartz (Q) framework grains, chlorite rims surrounding quartz grains (blue arrows), pore-filling clay (orange arrows), locally sutured grain contacts and stylolites (yellow arrows), and extensive pore-filling quartz cement (green arrows), along with minor amounts of heavy minerals (pink arrow). Pore spaces are impregnated with blue-dyed resin
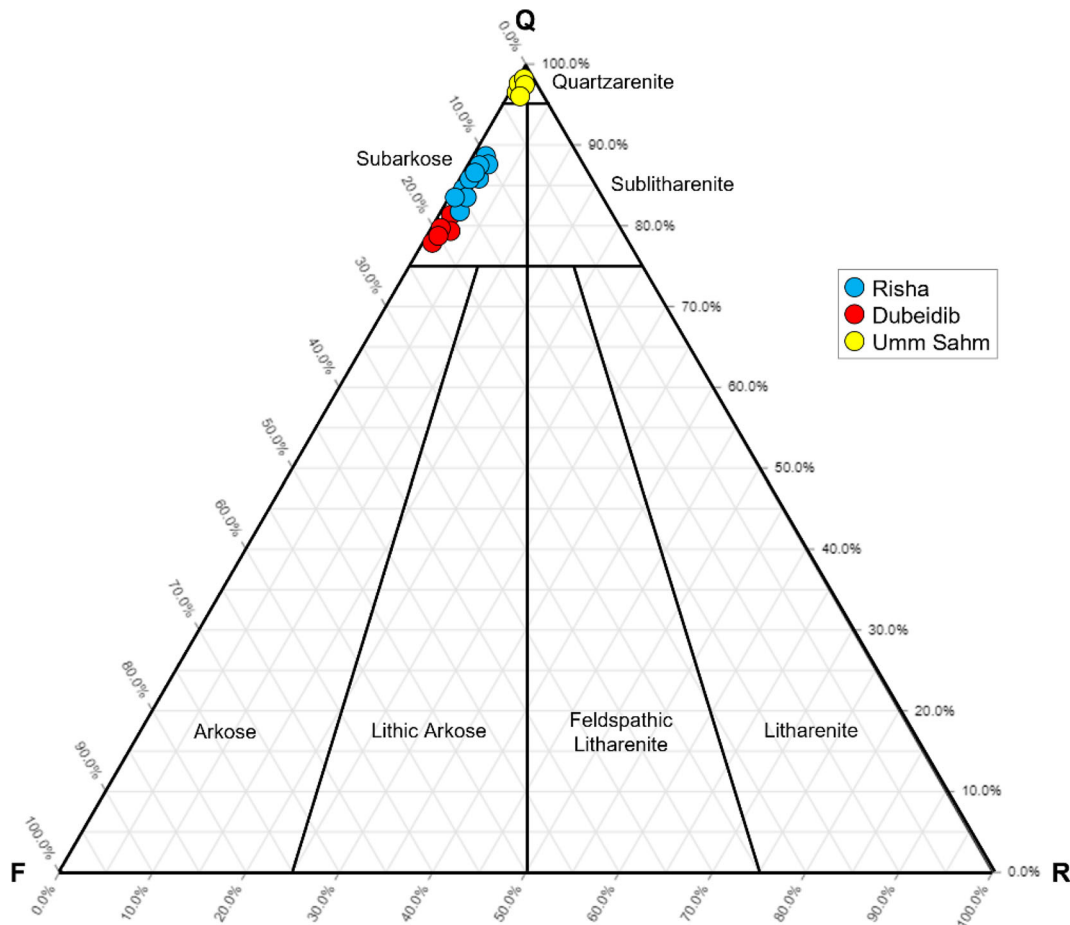

Fig. 21 QFR diagram showing the composition of the three studied sandstone reservoir intervals, constructed after Folk [44]. The plot shows that the Risha and Dubeidib sandstones are subarkose and the Umm Sahm sandstones are Quartz arenite

Springer
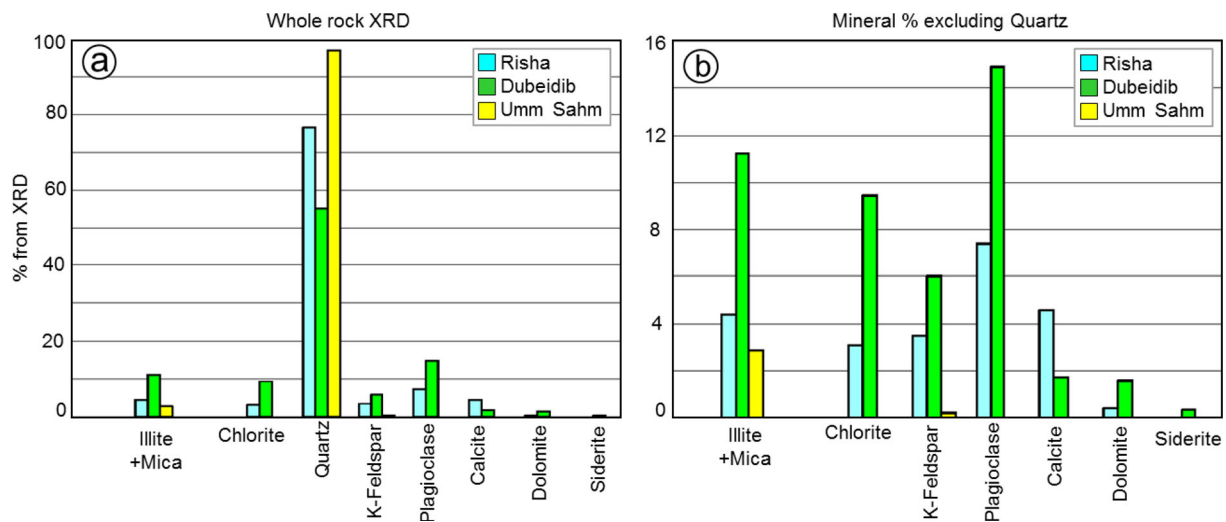
Fig. 22 a Whole-rock X-ray diffraction (XRD) results, and **b** mineral distributions excluding quartz from the Risha Formation (23 samples), Dubeidib Formation (7 samples), and Umm Sahm Formation (3 samples) in the Risha Field

Fig. 23 The paragenetic sequence of the main diagenetic features observed in the studied sandstones
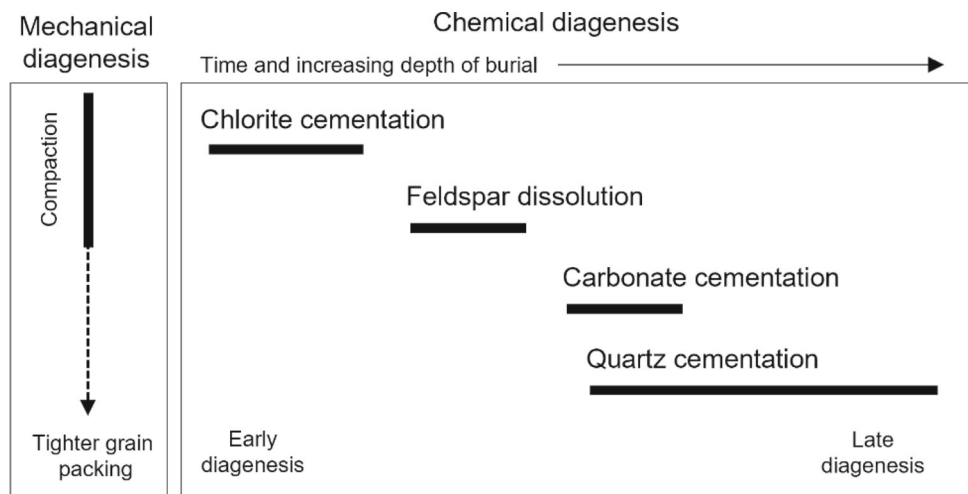

developed. Clay cementation is commonly observed in all the thin sections. Chlorite and illite are the dominant clay phases which can have authigenic or detrital origin. These clay minerals occur as pore-lining and pore-filling forms, as seen from thin sections as well as SEM images (Figs. 17d, 18a–c, 19b, and 20a–b). Chlorite mostly occurs as grain coatings surrounding the quartz framework grains in all three reservoirs, which are usually formed in the early diagenesis period [45, 46]. Such clay forms are extensively reported from clastic reservoirs globally [46–48].

Feldspar dissolution was observed in the thin section, which might have taken place during and immediately after the initial diagenetic phase. The occurrence of fresh as well as partially dissolved feldspar within the same reservoir may indicate pre-depositional weathering at the sediment source or post-depositional selective alteration [19, 20, 30]. Partial

dissolution of feldspar contributes to secondary porosity generation and may be considered a reservoir quality-enhancing diagenetic agent [49–51]. This effect was limited to the Risha and Dubeidib intervals, while the Umm Sahm Sandstone is almost devoid of feldspar (as seen from XRD, Fig. 21a–b). Cementation is observed as the dominant diagenetic factor. Thin sections and SEM images indicate extensive silica cementation and minor carbonate cementation in the pore spaces which significantly decreased the porosity and hence reservoir quality. Carbonate cement precipitation may occur in a shallow marine setting or during burial. The dolomites observed in the thin sections might have been formed from the precursor carbonate material by dolomitization facilitated by moderate burial. At the late diagenetic stage, silica cementation might have occurred in deep burial conditions. This is generally facilitated by higher temperature conditions [52],
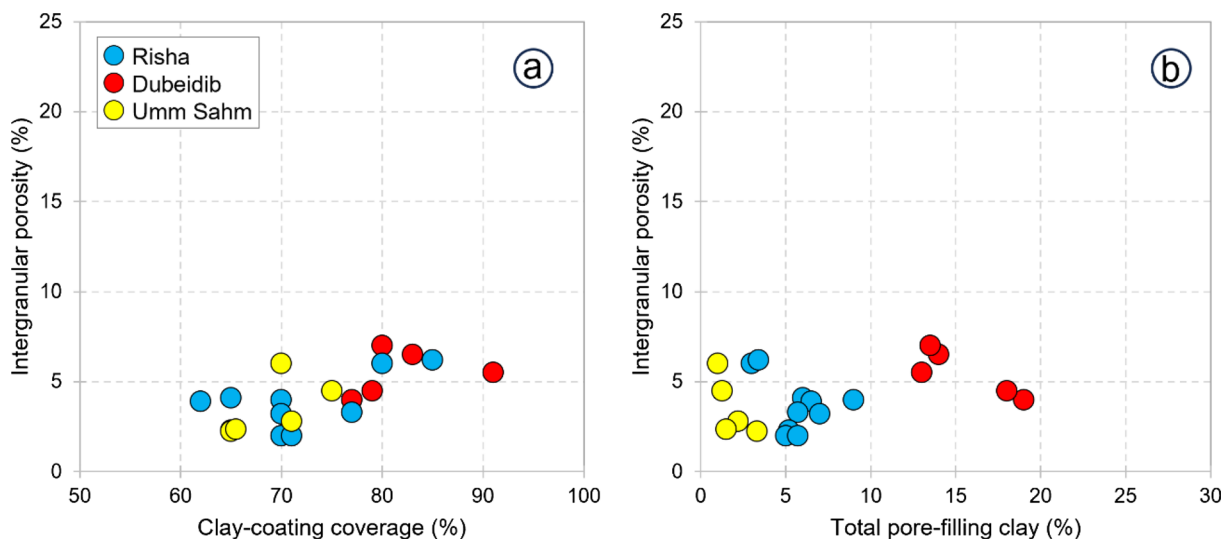
Fig. 24 Impact of clay-coating coverage and pore-filling clays on intergranular porosity. **a** plot of intergranular porosity against clay-coating coverage indicating a minor increase in intergranular porosity with increasing clay-coating coverage on detrital grains, **b** plot of intergranular porosity against total pore-filling clay indicating higher clay content in the Dubeidib sandstones
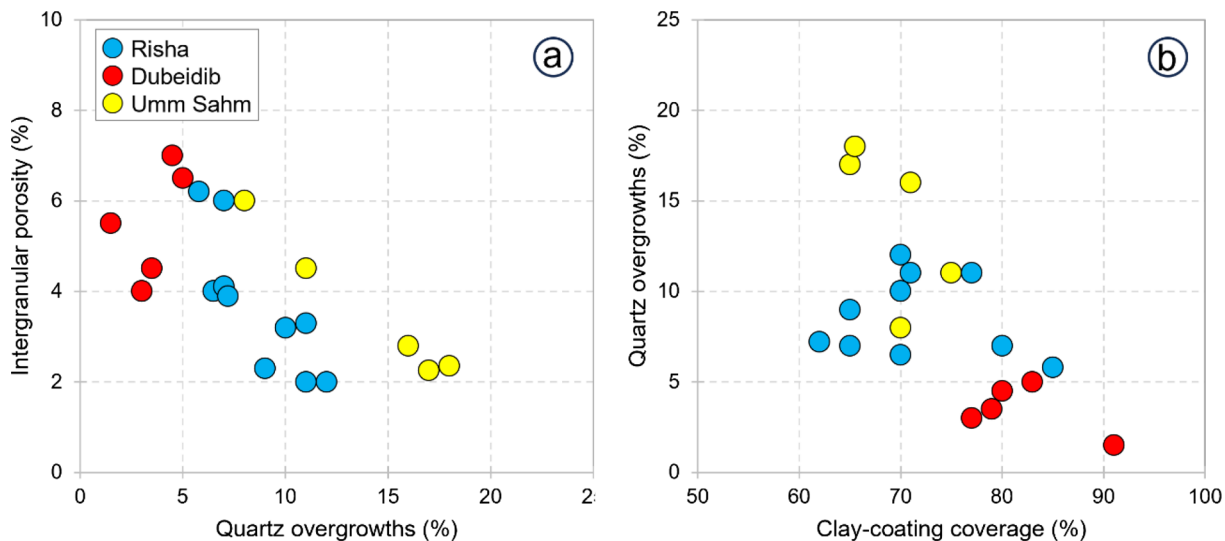
Fig. 25 Relation between quartz overgrowths with intergranular porosity and clay-coating coverage. **a** plot of intergranular porosity against quartz overgrowth indicating a decrease in intergranular porosity with increasing quartz cement volume, **b** plot of quartz overgrowth against clay-coating coverage indicating a decrease in quartz cement volume with increasing clay-coating coverage

but quartz dissolution and consequent availability for repre-cipitation also increase rapidly with temperatures above ~ 100 °C [53–55]. The Umm Sahm Sandstone exhibits long sutured grain contacts and stylolites indicating intense chemical compaction (Fig. 20a), and therefore pressure solution at the quartz grain contacts is possibly the major source of silica cement at the later stages of the diagenesis.

5.2 Effects of Diagenesis on Reservoir Quality

The two main diagenetic factors that influenced the studied reservoirs are clay cementation at the early diagenetic phase and silica cementation in the late diagenetic stage. The silica cementation negatively affects the reservoir porosity. However, the clay coatings can raise the reservoir's compressive strength [56] and hinder quartz overgrowths, and potentially reduce further porosity loss [50, 51, 57, 58]. To understand this effect, please refer to Figs. 24, 25 that

Fig. 26 Core photographs of calcite-filled thin natural fractures (marked by red arrows) within the studied **a** Risha Formation, well RH-25, depth 2653 m and **b** Umm Sahm Formation, well RH-47, depth 4004–4005 m from the Risha Field
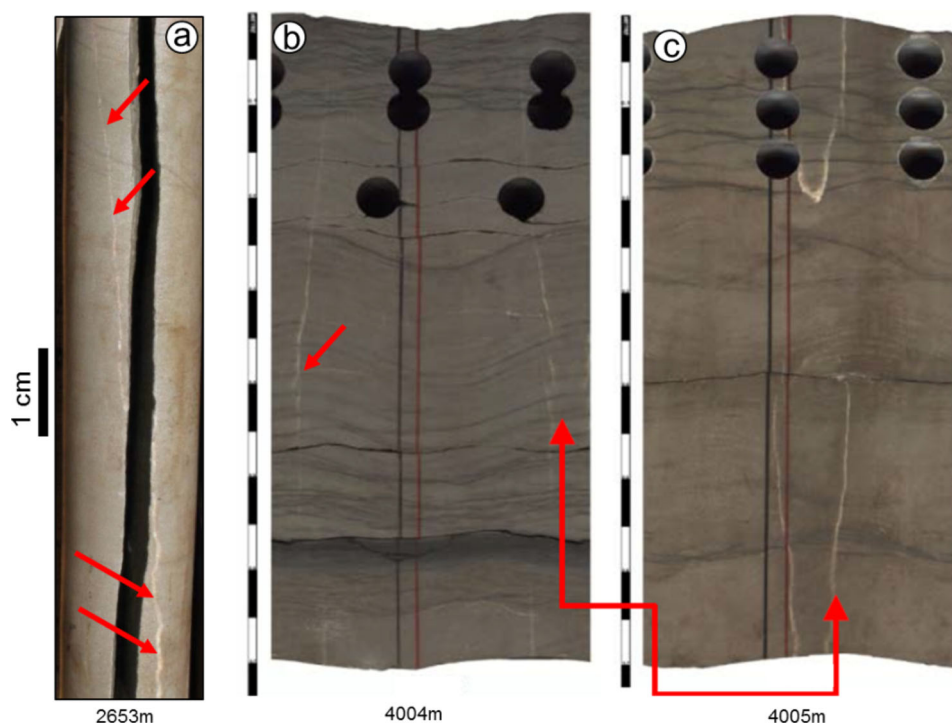

present the cross-plots using point count data in relation to the intergranular porosity. The cross-plot between clay-coating coverage (%) and intergranular porosity indicates a positive correlation where the samples with > 80% clay-coating coverage indicates the intergranular porosity of more than 5% (Fig. 24a), while the samples with higher clay-coating coverage exhibit strongly negative corelation with the quartz overgrowth by silica cementation (Fig. 25b). The Dubeidib Sandstone shows a higher clay-coating coverage of > 75% and these have a lower quartz overgrowth (< 5%), while the Umm Sahm Sandstone exhibits the highest quartz overgrowth (up to 18%), associated with lesser clay-coating coverage (< 75%) (Fig. 25b). Based on the point count data, the Dubeidib Sandstone samples exhibit the higher amount of total pore-filling clay up to 18%. Based on the 15 thin sections, we do not see a very strong correlation between total volume of pore-filling clay and intergranular porosity. However, due to the pore-filling habit, the clay minerals generally have a negative impact on the reservoir quality. The late diagenetic silica cementation shows a strongly negative correlation with reservoir porosity. The Risha and Umm Sahm Sandstones with quartz overgrowth of > 10% show intergranular porosity below 4% (Fig. 25a).

5.3 Petrophysical Quality and Reservoir Productivity—Inferences for Reservoir Development

The wireline log-based quantitative assessments indicate good reservoir petrophysical qualities in terms of shale volume and water saturation. The Paleozoic reservoirs are characterized by their clean nature (low shale volume, below 0.3 dec) and high hydrocarbon saturation ranging between 0.45 and 0.95 dec and dominantly above 0.75 dec. Gas effects are commonly observed in the petrophysical cross-plots (Figs. 12, 13 and 14). However, routine core analysis has determined very poor porosity (mostly < 5%) and tight permeability below 1 mD, dominated by micro- and meso-porosities (Fig. 3). Poor effective porosity was also observed from wireline log-based estimates, which is usually between 0.06 and 0.12 dec. Extensive silica cementation is the dominant diagenesis mechanism behind the tight nature of these gas-bearing sandstones. Feldspar dissolution did not have much positive effect on porosity enhancement.

We observed very thin high-angle fractures within the cores (Fig. 26a–c) of the Risha and Umm Sahm intervals. Open natural fractures generally provide efficient flow pathways in such tight reservoirs, however, the thin sub-vertical fractures seen on the cores are calcite-filled, and these calcite-filled fractures will not contribute much to the reservoir permeability. However, an open fracture network can be present locally which could significantly improve reservoir permeability.

Fig. 27 Mud loss events encountered during drilling through the Risha Formation from the wells RH-7 and RH-16
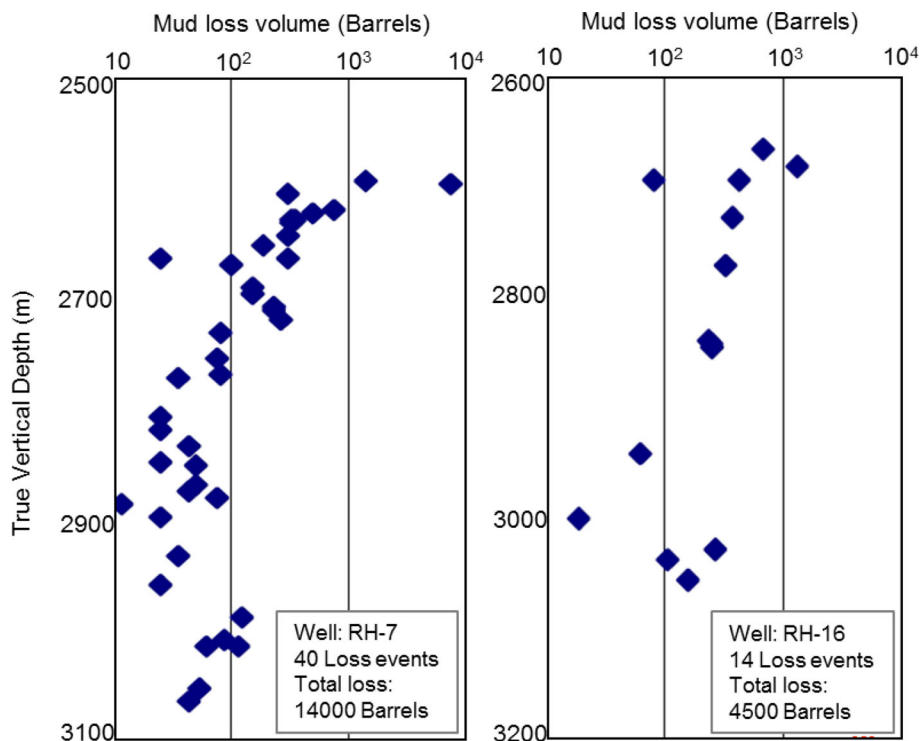
To understand the presence and role of fractures, we investigated the drilling history of some of the best-producing wells in the Risha gas field, i.e. RH-7 and RH-16. Partial mud loss events were reported from these two wells while drilling the Paleozoic Risha reservoir section. RH-7 experienced 40 loss events with a cumulative mud loss volume of around 14,000 barrels, while ~ 4500 barrel mud loss was reported from 14 events in the well RH-16 (Fig. 27). These observations indicate the possible presence of fractured intervals which contributed to the mud losses during drilling. The high productivity of these two wells (RH-7 and RH-6) confirms the presence of excellent permeability zones within the Risha interval.

Due to the unavailability of the wireline logs, the lithological interpretation of these two wells could not be presented. But the drilling report and mudlog indicates dominantly sandstone intervals with minor shale intercalation, which is a typical characteristic of the Risha Formation, as can be seen from the presented petrophysical logs of RH-3 (Fig. 4), RH-9 (Fig. 5), RH-46 (Fig. 6) and RH-57 (Fig. 7). The first loss events were encountered in the wells RH-7 and RH-46 at around 2600 and 2650 m, respectively (Fig. 23). The occurrence of first loss events confirms the presence of fractured intervals at those depths (2600 m in RH-7 and ~ 2650 m in RH-47). As losses continued while drilling the deeper section, it is difficult to confirm from the loss data if further fractured intervals are present below the first loss zone. Based on the drilling experienced, two subsurface scenarios are possible therefore: (i) Fractures are only present in the

zone where the first loss was reported, and that same interval consistently experienced mud loss while drilling further, and (ii) along with the first fractured interval (interval with first reported losses), there are multiple similar zones with fracture-enhanced permeability, which repeatedly exhibited multiple loss events. It is to be noted that the drilling data (loss depths and loss volumes) cannot alone confirm and identify all the potentially fractured zones. Image logs and production logging data are more suitable inputs to confirm the same. Mapping the fractured intervals and characterization of the fracture geometry is critical, especially while dealing with such tight sandstone reservoirs. We highly recommend running wireline image logging tools in the upcoming wells which would be able to capture such fractures.

6 Conclusions

This study characterizes the reservoir properties of the gas-bearing Cambro-Ordovician sandstones from the Risha field, Jordan. The quartz arenites and subarkosic reservoirs of the Risha, Dubeidib, and Umm Sahm formations exhibit high mineralogical maturity and moderate textural maturity. All the reservoirs are extensively affected by various diagenetic factors including cementation (dominantly silica, minor carbonate, and clay) and compaction (both mechanical and chemical) which reduce the reservoir storage and flow capacities. Petrophysically these are very tight with < 6% porosity and have very poor horizontal permeability (mostly

< 1 mD). However, low shale volume and excellent hydrocarbon saturation make these tight sandstones very good unconventional gas reservoirs, if necessary, completion techniques are applied. Drilling events in a few high-performance wells (in terms of production) indicate high-volume mud loss events, which might be caused by natural fractures. We highly recommend acquiring image log data in the upcoming wells which will provide a direct information about the geometries and effectiveness of any pre-existing fracture sets. The studied cores only show some thin sub-vertical fractures filled with calcite and these did not enhance the reservoir flow capacity. We envisage the possibility of permeability improvement within the studied tight Paleozoic reservoirs under the influence of natural or hydraulically created fractures. Necessary reservoir development strategies are discussed based on petrophysical and petrographical observations.

References

1. Khlaifat, A.; Qutob, H.; Barakat, N.: Increasing the world's gas reserves by the exploitation of unconventional tight gas reservoirs. In: SPE/PAPG Annual Technical Conference, Islamabad, Pakistan, 10–11 Nov. SPE-42842 (2010)

2. Holditch, S.: Tight gas sands. J. Pet. Technol. **58**(6), 86–93 (2006)

3. Kawata, Y.; Fujita, K.: Some predictions of possible unconventional hydrocarbons availability until 2100. In: SPE Asia Pacific Oil and Gas Conference and Exhibition, Jakarta, Indonesia, 17–19 Apr. SPE-68755 (2001)

4. Baouche, R.; Ganguli, S.S.; Sen, S.; Radwan, A.E.: Assessment of reservoir stress state and its implications for Paleozoic tight oil reservoir development in the Oued Mya Basin, northeastern Algerian Sahara. Geosyst. Geoenviron. **2**(1), 100112 (2023)

5. Baouche, R.; Sen, S.; Feriel, H.A.; Radwan, A.E.: Estimation of horizontal stresses from wellbore failures in strike-slip tectonic regime: a case study from the Ordovician reservoir of the Tinzaouatine Field, Illizi Basin Algeria. Interpretation **10**(3), SF37–SF44 (2022)

6. Baouche, R.; Sen, S.; Chaouchi, R.; Ganguli, S.S.: Modeling in-situ tectonic stress state and maximum horizontal stress azimuth in the Central Algerian Sahara—A geomechanical study from EL Agreb, EL Gassi and Hassi Messaoud fields. J. Nat. Gas Sci. Eng. **88**, 103831 (2021)

7. Bu-Khamseen, R.; Khakimov, A.; Sierra, L.; Young, D; Machala, M.: First successful tight gas reservoir completion and fracture stimulation in Sarah Formation, Rub Al-Khali Empty Quarter of Saudi Arabia. In: SPE Deep Gas Conference and Exhibition, Manama, Bahrain, January 2010, SPE-130722 (2010). https://doi.org/10.2118/130722-MS

8. Adebayo, A.R.; Babalola, L.; Hussaini, S.R.; Alqubalee, A.; Babu, R.S.: Insight into the pore characteristics of a Saudi Arabian tight gas sand reservoir. Energies **12**, 4302 (2019)

9. Naylor, D.; Al-Rawi, M.; Clayton, G.; Fitzpatrick, M.J.; Green, P.F.: Hydrocarbon potential in Jordan. J. Pet. Geol. **36**, 205–236 (2013)

10. Journal of Petroleum Technology (JPT). Jordan Finds "Promising" Gas Reserves Near Iraq Border. Report Dated Feb 1, 2021 (2021)

11. Sorkhabi, R.: Paleozoic tight gas plays in Jordan. GEO Expro. https://www.geoexpro.com/articles/2010/01/paleozoic-tight-gas-plays-in-jordan (2009)

12. Luning, S.; Kuss, J.: Petroleum geology of Jordan. In: Marlow, L., Kendall, C.C.G., Rose, L.A. (eds.) Memoir 106, Petroleum Systems of the Tethyan Region, pp. 217–239. AAPG Special Volume (2014)

13. Jordan Times (JT). Kharabsheh announces effort to drill 6 gas wells near Iraqi border. Report, Dated Dec 4, 2021 (2021)

14. Hirst, J.P.P.; Khatatneh, M.: Depositional model for the distal Ordovician glaciated margin of Jordan; implications for the reservoir potential of the Risha Formation. Geol. Soc. Lond. Spec. Publ. **475**(1), 109–129 (2019)

15. Abed, A.M.; Makhlouf, I.M.; Amireh, B.S.; Khalil, B.: Upper Ordovician glacial deposits in southern Jordan. Episodes **16**, 316–328 (1993)

16. Amireh, B.S.; Schneider, W.; Abed, A.M.: Fluvial-shallow marine-glaciofluvial depositional environments of the Ordovician System in Jordan. J. Asian Earth Sci. **19**, 45–60 (2001)

17. Amireh, B.S.; Schneider, W.; Abed, A.M.: Evolving fluvial-transitional-marine deposition through the Cambrian sequence of Jordan. Sed. Geol. **89**, 65–90 (1994)

18. Makhlouf, I.: Tempestite facies displaying hummocky cross-stratification and subaqueous channels in Ordovician shelf deposition, South Jordan. J. Afr. Geosci. Rev. **2**, 91–100 (1995)

19. Armstrong, H.A.; Abbott, G.D.; Turner, B.R.; Makhlouf, I.M.; Muhammad, A.B.; Pedentchouk, N.; Peters, H.: Black shale deposition in an Upper Ordovician–Silurian permanently stratified, peri-glacial basin, southern Jordan. Palaeogeogr. Palaeoclimatol. Palaeoecol. **273**(3–4), 368–377 (2009)

20. Armstrong, H.A.; Turner, B.R.; Makhlouf, I.M.; Williams, M.; Al Smadi, A.; Salah, A.A.: Sequence stratigraphy and depositional environment of an Upper Ordovician (Hirnantian), peri-glacial petroleum source rock. Palaeogeogr. Palaeoclimatol. Palaeoecol. **220**, 273–289 (2005)

21. Luning, S.; Shahin, Y.M.; Loydell, D.; Al-Rabi, H.T.; Masri, A.; Tarawneh, B.; Kolonic, S.: Anatomy of a world-class source rock: distribution and depositional model of Silurian organic-rich shales in Jordan and implications for hydrocarbon potential. AAPG Bull. **89**(10), 1397–1427 (2005)

22. Lüning, S.; Craig, J.; Loydell, D.K.; Štorch, P.; Fitches, B.: Lower Silurian hot shales in North Africa and Arabia: regional distribution and depositional model. Earth Sci. Rev. **49**(1–4), 121–200 (2000)

23. Turner, B.R.; Makhlouf, I.M.; Armstrong, H.A.: Late Ordovician (Ashgillian) glacial deposits in southern Jordan. Sed. Geol. **181**, 73–91 (2005)

24. Douilet, G.; Ghienne, J.-F.; Geraud, Y.; Abueladas, A.; Diraison, M.; Al-Zoubi, A.: Late Ordovician tunnel valleys in southern Jordan. In: Husse, M.; Redfern, J.; Le Heron, D.P.; Dixon, R.J.; Moscariello, A.; Craig, J. (Eds.) Glaciogenic Reservoirs and Hydrocarbon Systems, pp. 275–292. Geological Society, London (2012)

25. Ghienne, J.-F.; Desrochers, A., et al.: A Cenozoic style scenario for the end-Ordovician glaciation. Nat. Commun. **5**, 4485 (2014)

26. Farouk, S.; Faris, M.; Ahmad, F.; Powell, J.: New microplanktonic biostratigraphy and depositional sequences across the Middle-Late Eocene and Oligocene boundaries in eastern Jordan. Geology **20**(3), 145–172 (2015)

27. Hakimi, M.H.; Alqudah, M.; Mustapha, K.A.; Varfolomeev, M.A.; Lashin, A.; Hatem, B.A.; Rahim, A.; Sen, S.; Radwan, A.E.; Yelwa, N.A.: Early-oil generation potential of type II-S kerogen in the upper cretaceous (Cenomanian–Turonian) organic-rich carbonate succession from Ajloun region in Northern Jordan. Arab. J. Sci. Eng. **48**, 695–720 (2023)

28. El-Deek, I.; Abdullatif, O.; Korvin, G.: Heterogeneity analysis of reservoir porosity and permeability in the Late Ordovician glacio-fluvial Sarah Formation paleovalleys, central Saudi Arabia. Arab. J. Geosci. **10**, 400 (2017)

29. Lotfy, N.M.; Qteishat, A.; Farouk, S.; Ahmed, F.; Al-Kahtany, K.; Hsu, C.S.: Geochemical characteristics and genetic types of Ordovician tight gas in the Risha Gas Field, Eastern Jordan based on carbon and hydrogen isotope compositions. Mar. Pet. Geol. **143**, 105810 (2022)

30. Tamar-Agha, M.Y.: The influence of cementation on the reservoir quality of the Risha Sandstone Member (Upper Ordovician), Risha Gasfield, NE Jordan. J. Pet. Geol. **32**(2), 193–208 (2009)

31. Jacobs, J.; Thomas, R.J.: Himalayan-ype indenter-escape tectonics model for the southern part of the late Neoproterozoic-early Paleozoic East African-Antarctic region. Geology **32**(8), 721–724 (2004)

32. Kusky, T.M.; Matsah, M.I.: Neoproterozoic dextral faulting in the Najd Fault System, Saudi Arabia, preceded sinistral faulting and escape tectonics related to closure of the Mozambique Ocean. Geol. Soc. Lond. Spec. Publ. **206**, 327–361 (2003)

33. Laboun, A.A.: Paleozoic tectono-stratigraphic framework of the Arabian Peninsula. J. King Saud Univ. (Sci.) **22**, 41–50 (2010)

34. Farouk, S.; Lofty, N.M.; Qteishat, A.; Ahmad, F.; Shehata, A.M.; Al-Kahtany, K.; Hsu, C.S.: Source and thermal maturity assessment of the Paleozoic-Mesozoic organic matter in the Risha gas field, Jordan. Fuel **335**, 126998 (2023)

35. Powell, J.H.; Abed, A.M.; Le Nindre, Y.-M.: Cambrian stratigraphy of Jordan. GeoArabia **19**(3), 81–134 (2014)

36. Beydoun, Z.R.; Futyan, A.R.I.; Jawzi, A.H.: Jordan revisited: hydrocarbon habitat and potential. J. Pet. Geol. **17**, 177–194 (1994)

37. Senalp, M.A.; Al-Duaiji, A.A.: Qasim Formation: Ordovician Storm- and Tide-Dominated Shallow-Marine Siliciclastic Sequences, Central Saudi Arabia. GeoArabia (2001). https://doi.org/10.2113/geoarabia0602233

38. Sadooni, F.N.; Dalqamouni, A.: Geology and petroleum prospects of Upper Triassic sediments, Jordan. Mar. Pet. Geol. **15**, 783–801 (1998)

39. Lüning, S.; Loydell, D.K.; Storch, P.; Shahin, Y.; Craig, J.: Origin, sequence stratigraphy and depositional environment of an Upper Ordovician (Hirnantian) deglacial black shale, Jordan—Discussion. Palaeogeogr. Palaeoclimatol. Palaeoecol. **230**, 352–355 (2006)

40. Asquith, G.; Gibson, C.: Basic Well Log Analysis for Geologists: Methods in Exploration Series. AAPG, Tulsa (1982)

41. Poupon, A.; Leveaux, J.: Evaluation of water saturation in shaly formations. In: SPWLA 12th Annual Logging Symposium. Society of Petrophysicists and Well-Log Analysts (1971)

42. Dickson, J.A.D.: A modified staining technique for carbonates thin section. Nature **205**, 587–588 (1965)

43. Dutton, S.P.; Hutton, M.E.; Ambrose, W.A.; Childers, A.T.; Loucks, R.G.: Preservation of reservoir quality by chlorite coats in deep Tuscaloosa Sandstones, Central Louisiana, USA. Gulf Coast Assoc. Geol. Soc. **7**, 46–58 (2018)

44. Folk, R.L.: Petrology of Sedimentary Rocks. Hemphill Publishing Company, Austin (1980)

45. Lundegard, P.D.: Sandstone porosity loss; a" big picture" view of the importance of compaction. J. Sediment. Res. **62**(2), 250–260 (1992)

46. Freiburg, J.T.; Ritzi, R.W.; Kehoe, K.S.: Depositional and diagenetic controls on anomalously high porosity within a deeply buried CO_2, storage reservoir—the Cambrian Mt. Simon sandstone, Illinois basin, USA. Int. J. Greenh. Gas Control **55**, 42–54 (2016)

47. Dowey, P.J.; Hodgson, D.M.; Worden, R.H.: Pre-requisites, processes, and prediction of chlorite grain coatings in petroleum reservoirs: a review of subsurface examples. Mar. Pet. Geol. **32**, 63–75 (2012)

48. Zhu, S.; Wang, X.; Qin, Y.; Jia, Y.; Zhu, X.; Zhang, J.; Hu, Y.: Occurrence and origin of pore-lining chlorite and its effectiveness on preserving porosity in sandstone of the Middle Yanchang Formation in the Southwest Ordos basin. Appl. Clay Sci. **148**, 25–38 (2017)

49. Al-Juboury, A.; Howard, J.P.; Vincent, S.J.; Nichols, G.: Petrography, diagenesis and geochemistry f the Cambro-Ordovician Khabour sandstones, western Iraq: implications for reservoir quality and impact of the Hirnantian glaciation. Mar. Pet. Geol. **123**, 104733 (2021)

50. Bello, A.M.; Al-Ramadan, K.; Babalola, L.O.; Alqubalee, A.; Amao, A.O.: Impact of grain-coating illite in preventing quartz cementation: example from permo-carboniferous sandstone, Central Saudi Arabia. Mar. Pet. Geol. **149**, 106073 (2023)

51. Bello, A.M.; Jones, S.; Gluyas, J.; Acikalin, S.; Cartigny, M.: Role played by clay content in controlling reservoir quality of submarine fan system, Forties Sandstone Member, Central Graben, North Sea. Mar. Pet. Geol. **128**, 105058 (2021)

52. Lai, J.; Wang, G.; Chai, Y.; Xin, Y.; Wu, Q.; Zhang, X.; Sun, Y.: Deep burial diagenesis and reservoir quality evolution of high-temperature, high-pressure sandstones: examples from Lower Cretaceous Bashijiqike Formation in Keshen area, Kuqa depression, Tarim basin of China. AAPG Bull. **101**(6), 829–862 (2017)

53. Rimstidt, J.D.: Quartz solubility at low temperatures. Geochim. Cosmochim. Acta **61**(13), 2553–2558 (1997)

54. Worden, R.H.; Morad, S.: Quartz cementation in oil field sandstones: a review of the key controversies. In: Worden, R.H.; Morad, S. (Eds.) Quartz Cementation in Sandstones, pp. 1–20. Blackwell Science, Oxford (2000)

55. Bjørlykke, K.: Pore water flow and mass transfer of solids in solution in sedimentary basins. In: Parker, A.; Sellwood, B.W. (Eds.) Quantitative Diagenesis: Recent Developments and Applications to Reservoir Geology, pp. 189–221. Kluwer, Dordrecht (1994)

56. Spinelli, G.A.; Mozley, P.S.; Tobin, H.J.; Underwood, M.B.; Hoffman, N.W.; Bellew, G.M.: Diagenesis, sediment strength, and pore collapse in sediment approaching the Nankai Trough subduction zone. GSA Bull. **119**(3–4), 377–390 (2007)

57. Nguyen, B.T.T.; Jones, S.J.; Goulty, N.R.; Middleton, A.J.; Grant, N.; Ferguson, A.; Bowen, L.: The role of fluid pressure and diagenetic cements for porosity preservation in Triassic fluvial reservoirs of the Central Graben, North Sea. AAPG Bull. **97**(8), 1273–1302 (2013)

58. Cui, Y.; Wang, G.; Jones, S.J.; Zhou, Z.; Ran, Y.; Lai, J.; Li, R.; Deng, L.: Prediction of diagenetic facies using well logs—a case study from the Upper Triassic Yanchang Formation, Ordos Basin, China. Mar. Pet. Geol. **81**, 50–65 (2017)